Wu *et al. Energy Mater.* **2025**, *5*, 500027
DOI: 10.20517/energymater.2024.66

Energy Materials

Review

Open Access

Recent advances in functionalized separators for shuttle-free and dendrite-free lithium/sodium-sulfur batteries

Yu Wu[1], Jinri Huang[1], Ziheng Zhang[1], Daiqian Chen[1], Hesheng Yu[1], Fei Ma[2], Xiaojuan Zhang[3,*], Yuanfu Chen[1,4,*]

[1]School of Integrated Circuit Science and Engineering, and State Key Laboratory of Electronic Thin Films and Integrated Devices, University of Electronic Science and Technology of China, Chengdu 610054, Sichuan, China.
[2]School of Materials Science and Engineering, Southwest Jiaotong University, Chengdu 610031, Sichuan, China.
[3]Department of Field Medical Equipment, Daping Hospital, Army Medical University, Chongqing 400042, China.
[4]Yangtze Delta Region Institute (Huzhou), University of Electronic Science and Technology of China, B1 Building, Science and Technology Innovation Complex, Huzhou 313001, Zhejiang, China.

***Correspondence to:** Dr. Xiaojuan Zhang, Department of Field Medical Equipment, Daping Hospital, Army Medical University, No. 10 Changjiang Branch Road, Daping Street, Yuzhong District, Chongqing 400042, China. E-mails: zhangxj612@tmmu.edu.cn; Dr. Yuanfu Chen, School of Integrated Circuit Science and Engineering, and State Key Laboratory of Electronic Thin Films and Integrated Devices, University of Electronic Science and Technology of China, No. 2006, Xiyuan Ave, West Hi-Tech Zone, Chengdu 610054, Sichuan, China; Yangtze Delta Region Institute (Huzhou), University of Electronic Science and Technology of China, B1 Building, Science and Technology Innovation Complex, No. 819 Xisaishan Road, Huzhou 313001, Zhejiang, China. E-mails: yfchen@uestc.edu.cn

How to cite this article: Wu, Y.; Huang, J.; Zhang, Z.; Chen, D.; Yu, H.; Ma, F.; Zhang, X.; Chen, Y. Recent advances in functionalized separators for shuttle-free and dendrite-free lithium/sodium-sulfur batteries. *Energy Mater.* **2025**, *5*, 500027. https://dx.doi.org/10.20517/energymater.2024.66

Received: 30 Jun 2024 **First Decision:** 29 Jul 2024 **Revised:** 17 Aug 2024 **Accepted:** 28 Aug 2024 **Published:** 17 Jan 2025

Academic Editors: Jiazhao Wang, Jinqiang Zhang **Copy Editor:** Fangling Lan **Production Editor:** Fangling Lan

Abstract

With the extremely high theoretical energy densities, secondary batteries including lithium-sulfur (Li-S) and sodium-sulfur (Na-S) batteries are anticipated to become the leading candidates among metal-sulfur batteries. However, the practical energy density and storage efficiency of Li/Na-sulfur batteries are significantly hindered by several issues: the low conductivity of sulfur cathodes, substantial volume changes during charge and discharge cycles, the shuttle effect caused by metal polysulfides, and uncontrollable dendrite formation on the reactive alkali metal anodes, which also heighten safety concerns. Constructing functionalized separators is considered one of the most promising strategies to overcome these challenges and enhance the performance of Li/Na-sulfur batteries. Functionalized separators offer numerous advantages such as enhanced mechanical stability, bifunctionality in suppressing the shuttle effect and dendrite growth, and minimal impact on battery energy density and volume.

However, comprehensive reviews of Li/Na-sulfur functionalized separators are relatively fewer, while the related research has increased significantly. In this context, it is crucial to provide a comprehensive review of recent advances in functionalized separators for Li/Na-sulfur batteries. First, this review offers an in-depth analysis of the current issues faced by Li/Na-sulfur batteries and summarizes the requirements of separators for improving Li/Na-sulfur batteries. Subsequently, a detailed discussion is presented about the performances and applications especially in shuttle effect inhibition and dendrite growth suppression of functionalized separators in Li-S and Na-S batteries. Finally, the review addresses the challenges and potential future research directions for functionalized separators in Li/Na-sulfur batteries.

Keywords: Li-S battery, Na-S battery, functionalized separators, polysulfide shuttle inhibition, dendrite growth suppression

INTRODUCTION

Secondary batteries, with the higher capacity, fast charge-discharge rates, long lifespan, and environmental friendliness, not only have strong competitiveness in replacing traditional fossil fuels such as coal and oil as powerful renewable energy devices, but are also crucial for the development and storage of renewable energy sources such as wind and hydrogen energy. Alkali metal, with high theoretical specific capacity, low density and electropositive potential, has quickly become the preferred choice for the anode of high-energy-density storage systems. The batteries taking alkali metals as anodes are widely used to meet the strong demand for large-scale and portable energy solutions, such as new energy vehicles, power storage, and power supply sectors. Among them, lithium-ion batteries (LIBs) stand out due to the advantages of lightweight, long lifespan, low self-discharge, minimal pollution, weak memory effect, and high energy density. Since the initial commercialization in 1991, LIBs have gradually replaced traditional primary batteries and are widely used in portable electronic devices. However, the practical energy density of LIBs, based on intercalation reaction mechanism, has nearly reached its theoretical limit, making it difficult to meet current energy storage demands[1]. Therefore, there lies an urgent need to develop a new generation of secondary batteries with higher capacity and energy density, as well as safety, eco-friendliness, and economic viability[2].

Metal-sulfur batteries using alkali metals as the anode and sulfur or sulfur-based composite materials as the cathode are considered one of the most promising next-generation batteries to replace LIBs. The redox reaction of the sulfur cathode involves multi-electron transfer, resulting in a high theoretical specific capacity of up to 1,672 mAh g^{-1}. Additionally, the reaction energy between sulfur and alkali metals is relatively high, providing a high theoretical energy density far exceeding that of LIBs. Furthermore, compared to the commonly used cathode materials in traditional LIBs, such as lithium cobalt oxide or lithium iron phosphate, sulfur has a lower molecular weight and is abundantly available in the Earth's crust, ensuring the economic viability of metal-sulfur batteries. Among these, lithium-sulfur (Li-S) batteries using lithium metal as the anode, with its small atomic weight and high electrochemical activity, have the highest theoretical energy density of all metal-sulfur batteries, reaching up to 2,600 Wh kg^{-1}, approximately seven times that of LIBs. Coupled with a relatively low operating voltage (2.1 V), Li-S batteries hold great potential for applications requiring safe, lightweight, and long-lasting energy storage solutions. Additionally, sodium-sulfur (Na-S) batteries, which have been in commercial use since 1992, utilize sodium from the same group as lithium as the anode. Although the theoretical energy density of Na-S batteries (760 Wh/kg) is lower than that of Li-S batteries, the abundant and inexpensive nature of sodium significantly reduces the cost of these batteries[3]. The higher chemical stability of sodium also provides relatively higher safety. Moreover, Na-S batteries exhibit long cycle life at high temperatures, making them particularly advantageous for use in stationary energy storage systems.

Unfortunately, Li-S and Na-S batteries face some unique challenges compared to LIBs. On the one hand, the low conductivity of sulfur cathodes, volume changes caused by phase transformations during the charge-discharge cycle, and the polysulfide "shuttle effect" post huge threat to the practical energy density and storage efficiency of Li/Na-sulfur batteries. On the other side, the chemically reactive nature of Li/Na anodes leads to uncontrolled dendrite growth due to uneven deposition, which can pierce the separator, causing short circuits and safety issues. Compared to Li-S batteries, Na-S batteries suffer from slower sodium anode reaction kinetics and fewer suitable electrolyte materials. Overall, the poor conductivity of active materials, large volume changes, and, most importantly, the shuttle effect of polysulfides and uncontrollable dendrite growth of anode severely constrain the practical application of Li/Na-sulfur batteries[4].

In this case, some strategies such as electrode design, electrolyte optimization, and separator modification are proposed and applied as the primary engineering approaches for improving Li/Na-sulfur batteries[5,6]. Enhancing the conductivity and microstructure of the sulfur cathode can increase sulfur utilization and loading while mitigating the impacts of volume changes, thereby improving the cycling performance of Li/Na-sulfur batteries[7-9]. Synthesizing alloy anode materials or constructing protective layers or artificial solid electrolyte interphase (SEI) on the anode surface can enhance the stability of the metal anode, reduce lithium dendrite growth, and improve the safety and cycling life of Li/Na-sulfur batteries[10]. However, electrode modification techniques often address specific problems on one side of the electrode, and dual electrode modification can significantly increase the production cost of Li/Na-sulfur batteries. Electrolyte optimization strategies primarily focus on developing functional additives and solid-state electrolytes. However, the complexity and uncontrollability of electrochemical reactions at the electrolyte-electrode interface remain to be the most challenging issues[11,12]. The separator, directly contacting the cathode and anode, plays a crucial role in substantial transfer processes at the S cathode and metal anode interfaces, particularly in polysulfide diffusion and metal ion migration[13]. Functional modification of separators helps enhance the adsorption of polysulfides, accelerate the conversion between different forms of polysulfides during charge/discharge reactions, and alleviate the resulting cathode volume changes, which accelerates cathode reaction kinetics and suppresses the shuttle effect. Functionalized separators are also able to contribute to regulating the uniformity of metal lithium/sodium ion flux and assist in the formation of a stable SEI layer, thereby inhibiting dendrite growth[14,15]. Additionally, separator modification can improve battery cycling performance without significantly sacrificing the energy density, volume, or weight of Li/Na-sulfur batteries. Therefore, whether implemented as an independent or combined strategy, separator modification is one of the most promising and effective approaches. Developing green, cost-effective multifunctional separators is also a crucial means to promote the commercialization of Li-S and Na-S batteries.

This review provides an in-depth discussion of the design principles and application strategies of functionalized separators for Li-S and Na-S batteries, particularly in inhibiting the polysulfide shuttle and uncontrolled metal dendrite growth, as illustrated in Scheme 1. First, the current issues faced by Li-S and Na-S batteries were analyzed, focusing on the mechanisms of polysulfide conversion processes and the associated shuttle effect, as well as the nucleation and growth of dendrites on the reactive alkali metal anode. Next, the roles, strategies, and principles of functionalized separators in achieving the bifunctionality of suppressing the shuttle effect and dendrite growth were thoroughly introduced. Then, comprehensive reviews were presented about the progress of the research toward functionalized separators designed based on different working principles for Li-S and Na-S batteries. Finally, overall conclusions and future perspectives were given on the application of functionalized separators in Li/Na-sulfur batteries. This work provides a comprehensive framework for designing effective functionalized separators for metal-sulfur batteries, particularly bifunctional separators.

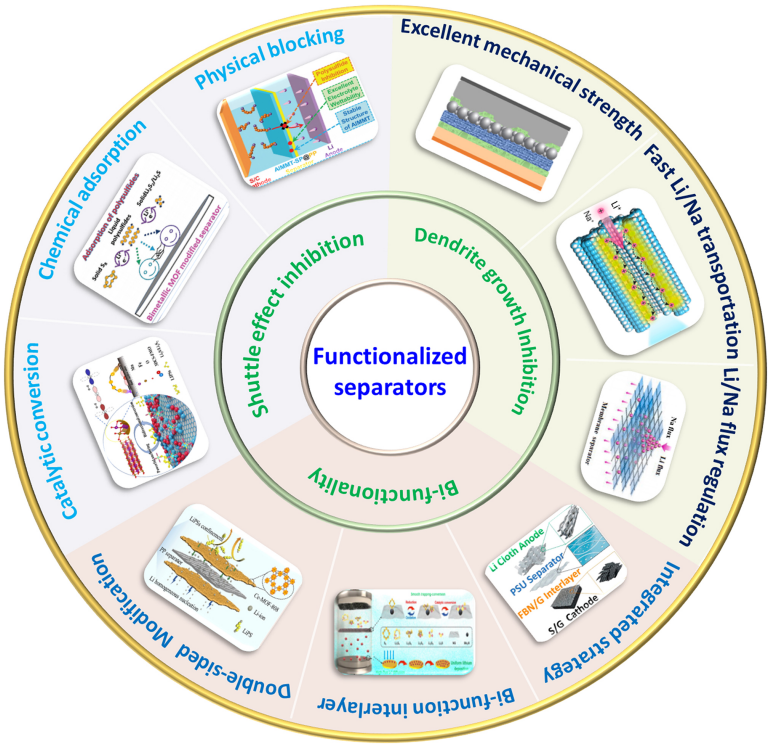

Scheme 1. Topics outline of this review.

CURRENT ISSUES AND STRATEGIES OF LI/NA-SULFUR BATTERIES

Current issues

Despite the extremely high energy density, Li/Na-sulfur batteries have long been hindered in practical applications due to unstable cycle life and performance, and serious safety issues. Therefore, a thorough analysis of the current challenges faced by Li/Na-sulfur batteries is crucial for proposing effective strategies to improve performance.

For the cathode, the poor conductivity of sulfur in Li/Na-S batteries limits the electron transport, reducing battery rate and capacity performances. During cycling, sulfur undergoes volume changes due to solid-liquid-solid phase transformations, weakening the electrode's mechanical stability and causing active material detachment. Additionally, polysulfides (Li_2S_n, $2 \le x \le 8$) dissolve in the electrolyte and migrate to the anode, leading to self-discharge, active material loss, and deteriorated battery cycling life[16]. For Li/Na metal anodes, uneven ion deposition during cycling leads to the formation of Li/Na dendrites, risking separator piercing and causing internal short circuits, fire, or explosion, as shown in Figure 1A[4,17]. Similar to the S cathode, Li/Na anodes undergo volume changes, creating surface cracks and defects, which increase mechanical stress and degrade electrode structure. The high reactivity of Li and Na worsens dendrite growth and side reactions, reducing cycle life and battery stability. The main challenges remain the polysulfide shuttle effect and metal dendrite growth. Generally, the shuttle effect of polysulfides of the S cathode side and the dendrite growth of the Li/Na anode are the most important and challenging issues for Li-S and Na-S batteries.

Shuttle effect of Li/Na polysulfide

The discharge process of Li/Na-sulfur batteries involves the reduction of sulfur (S_8) to polysulfides (Li_2S_n, $2 \le n \le 8$) and the release of electrons and Li^+, accompanied by solid-liquid-solid phase conversions. The

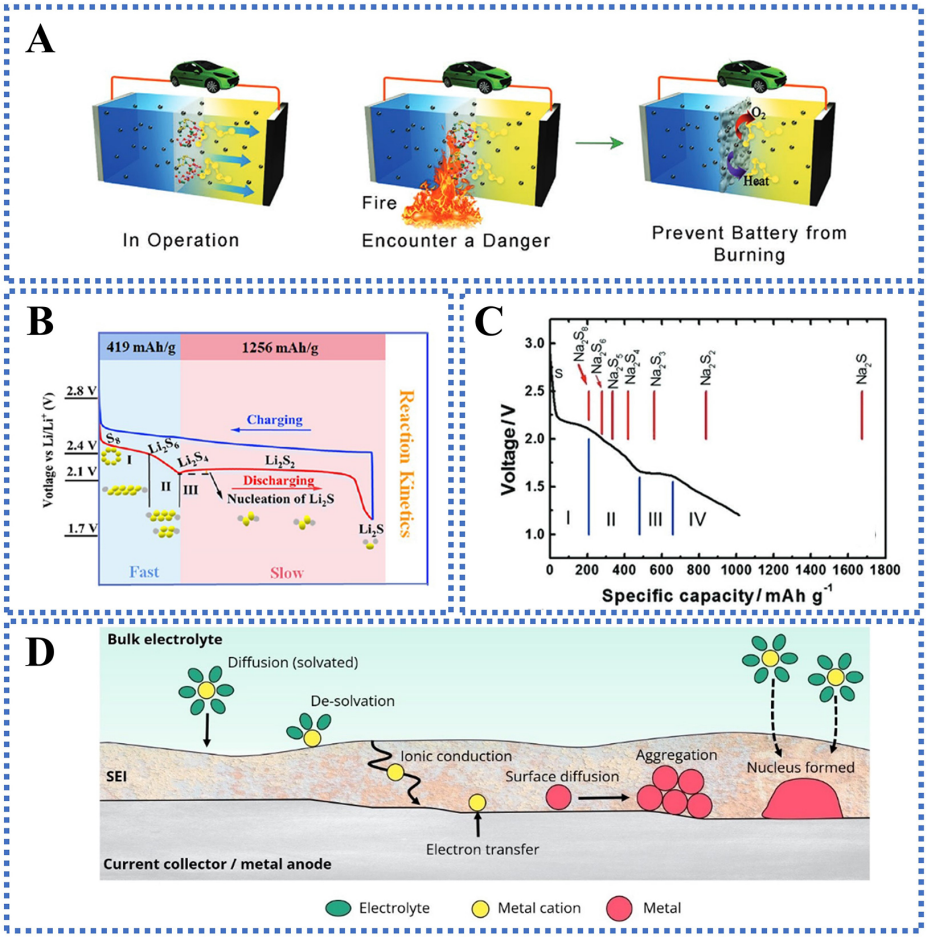

Figure 1. Current issues of Li/Na-sulfur batteries. (A) Schematics of the issues faced by Li-S batteries. (B) Theoretical charging/discharging profile of Li-S battery. (C) Theoretical discharge profile of Na-S battery. (D) Schematic illustration of the redox reactions on metal anode surface. This figure is quoted with permission from Lei *et al.*[4], Wu *et al.*[18], Yu *et al.*[20], and Cooper *et al.*[23], respectively.

typical discharge reaction of Li-S batteries is recognized as four stages as follows as shown in Figure 1B[18].

Stage I: The solid-phase S_8 ring in the cathode is reduced to Li_2S_8. This involves the solid-to-liquid conversion and the dissolution of polysulfides in the electrolyte, with the reaction plateau voltage above 2.4 V given in

$$S_8 + 2Li^+ + 2e^- \rightarrow Li_2S_8 \quad (1)$$

In stage II, Li_2S_8 migrates to the surface of the lithium metal anode under the influence of chemical diffusion and electric field forces and is reduced stepwise to higher-order polysulfides Li_2S_n ($4 \leq n \leq 8$) as given in

$$Li_2S_8 + 2Li^+ + 2e^- \rightarrow 2Li_2S_4 \quad (2)$$

$$3Li_2S_8 + 2Li^+ + 2e^- \rightarrow 4Li_2S_6 \quad (3)$$

$$2Li_2S_6 + 2Li^+ + 2e^- \rightarrow 3Li_2S_4 \quad (4)$$

During this stage, the transformation of polysulfides occurs entirely in the electrolyte, accompanied by a voltage plateau drop from approximately 2.4 to 2.1 V.

The stage III involves the conversion of soluble Li_2S_4 to insoluble lower-order polysulfides Li_2S_n ($1 \leq n \leq 3$), expressed as

$$Li_2S_4 + 2Li^+ + 2e^- \rightarrow 2Li_2S_2 \quad (5)$$

$$Li_2S_4 + 6Li^+ + 6e^- \rightarrow 4Li_2S \quad (6)$$

The stage IV refers to the solid-solid conversion of insoluble Li_2S_2 to Li_2S as

$$Li_2S_2 + 2Li^+ + 2e^- \rightarrow 2Li_2S \quad (7)$$

The last two stages, III and IV, are the slowest in terms of reaction kinetics during discharge because of the involvement of solid-state conversions[19]. Similarly, during the discharge process of Na-S batteries, a similar solid-liquid-solid transformation from $S_8 \rightarrow Na_2S$ occurs as shown in Figure 1C, similar to that in Li-S batteries[20]. The subsequent charging reaction of Li-S/Na-S batteries involves a multi-step reverse conversion from Li_2S/Na_2S to S_8.

The "shuttle effect" in Li/Na-S batteries occurs when soluble high-order polysulfides pass through conventional separators and reach the anode, reacting with Li/Na metal to form insoluble lower-order polysulfides (Li_2S_n/Na_2S_n, $1 \leq n \leq 3$)[21]. During charging, the lower-order polysulfides are unable to be oxidized back into higher-order forms and return to the cathode, leading to the accumulation on the anode as "dead sulfur". The shuttle effect of Li/Na polysulfides causes active material loss and increased irreversible capacity, reducing the practical capacity of Li/Na-sulfur batteries. Enhancing polysulfide adsorption and accelerating the conversion via physical/chemical methods are effective strategies to suppress the shuttle effect and improve battery performance. It is noteworthy that the formation and shuttle behavior of polysulfides in Na-S batteries exhibit significant differences compared to Li-S batteries. On the one hand, due to the larger ionic radius of Na^+, the complete discharge process from S_8 to Na_2S brings more severe volume expansion to the cathode, leading to increased issues of active material detachment and degradation (157% in Na-S batteries, compared to 80% in Li-S batteries)[22]. On the other hand, the weaker interaction between Na^+ and sulfide anions, derived from the lower electronegativity of Na^+, results in decreased interfacial stability and slower reaction kinetics, exacerbates the accumulation of soluble polysulfides and intensifies the shuttle effect.

Uncontrollable growth of Li/Na dendrites

For Li/Na-sulfur batteries, uneven Li/Na ion deposition results in the formation of "dead lithium" and "dead sodium", which are unable to participate in future electrochemical reactions, and aggravate undesirable metal dendrite growth on the surface of alkali metal anodes, as shown in Figure 1D[23]. The dendrites are prone to penetrate the separator, leading to short circuits, which not only reduce battery lifespan but also pose severe safety risks, including overheating and fire hazards[24].

The Sand's time model is widely applied for studying the formation and growth mechanism of metal dendrites. Taking Li-S batteries for instance, the concentration of Li^+ near the anode surface gradually decreases as the migration of Li^+ towards the cathode. When the Li^+ concentration reaches near zero at a specific current density, the formation of dendrites will be initiated, which is closely related to the Sand's

time, as given in[25]

$$\tau = \pi D \left(\frac{eC_o}{2Jt_a}\right)^2 \quad (8)$$

where J represents the effective electrode current density, D denotes the ambipolar diffusion coefficient, e is the electron charge, t_a stands for the anionic transference number, and C_o refers to the initial Li salt concentration.

At high current densities, the rate of Li^+ diffusion lags behind that of electroplating, leading to local supersaturation and uneven deposition, which triggers dendrite formation[26]. Continuous Li^+ deposition at the dendrite tips during cycling accelerates dendrite growth and threatens Li-S battery safety. According to Eq. (8), the nucleation time of metal dendrites inversely correlates with the current density J and directly with the Li^+ transference number t_{Li+} (which refers to 1-t_a). Thus, reducing local current density and increasing ion transference is vital for controlling dendrite growth.

In summary, during Li-S battery charging, Li^+ deposition on the anode is greatly affected by current density, surface energy, and electrode interface non-uniformity, leading to localized lithium deposition and dendrite formation. Accumulated Li in protruding areas enhances the local electric field, promoting further Li^+ deposition and accelerating dendrite growth. Additionally, the SEI layer formed during initial charging often has structural and compositional inconsistencies, causing uneven Li^+ conduction, SEI rupture, and further dendrite growth, which results in irreversible capacity loss and safety risks. In Na-S batteries, the sodium dendrites share almost similar formation and growth progress to lithium dendrites. However, the lower surface and adsorption energies of Na metal make uniform nucleation more difficult. Additionally, the lower chemical and electrochemical stability of Na^+ during high-current discharging exacerbates conductive pathway disruption and uncontrolled dendrite growth, leading to rapid degradation of battery performance. Thus, designing functional separators to inhibit sodium dendrite growth is more challenging than in Li-S batteries.

Strategies

General strategies

Common optimization strategies for Li/Na-S batteries include cathode and anode modification, electrolyte optimization, and separator functionalization[27]. Cathode improvements focus on enhancing conductivity and rigidity through physical regulation, chemical intercalation, and redox mediators, which aid sulfur redox reactions and manage volume changes[28]. Anode modifications encompass the development of three-dimensional (3D) anodes and artificial SEI layers. Electrolyte optimization, particularly in Na-S batteries, emphasizes solid-state electrolytes to address compatibility issues with Na metal[29].

Functionalized separator strategies

In Li/Na-S batteries, the separator contacts the sulfur cathode, Li/Na anode, and electrolyte, playing a key role in electrochemical reactions and ion transport[30]. The strategy towards functionalized separators with enhanced mechanical strength, regulated ion and molecular transport and suppressed shuttle effects and dendrite growth[15]. Traditional polypropylene (PP) and polyethylene (PE) separators exhibit poor mechanical properties, making them inadequate for handling electrode volume changes. The large, irregular pore sizes allow uncontrolled polysulfide diffusion, leading to capacity loss derived from the shuttle effect, and uneven ion deposition, causing dendrite growth. Current separator functionalization strategies include replacing separators with novel ones, adding functional layers, and integrating separator functionalization

with electrode and electrolyte modifications[31].

(a) Replacement of conventional separators

Polymer separators, including polyvinylidene fluoride (PVDF), polytetrafluoroethylene (PTFE), polyimide (PI), and polyacrylonitrile (PAN), are common alternatives to PP and PE separators. PVDF offers chemical stability and electrolyte wettability but lacks mechanical strength[32]. PI provides strong mechanical properties and thermal stability, but the application is limited by the high cost[33]. Similarly, the inferior economic efficiency of PTFE restricts its widespread application despite the stability advantages[34]. PAN is relatively competitive due to its mechanical strength, flexibility, and wettability but still requires further functionalization[35].

Glass fiber (GF) separators are promising separator alternatives due to their high porosity, thermal stability, electrolyte wettability, and electrochemical performance[36]. Although multifold thicker than PP, GF offers significant advantages in mechanical strength, electrolyte uptake, and ion transport, enhancing polysulfide capture and metal ion transport, and is particularly suited for Na-S batteries due to the superior porosity[37]. However, the thickness of GF separators, generally reaching over 100 μm, adds extra volume to the battery.

(b) Functional interlayer loading

Loading functional interlayers on commercial separators effectively regulates polysulfide diffusion and metal deposition and is efficient for achieving bifunctionality in suppressing the shuttle effect and dendrite growth. Interlayers can generally be categorized into double-sided loading and single-sided bifunctional material loading.

(i) Double-sided loading separators include sandwich and Janus types. Sandwich separators have functional materials on both the cathode and anode sides with the insulating membrane in the middle, while Janus separators consist of only two functional layers. On the cathode side, functional materials typically feature strong electronegativity, abundant polar bonds, nanoscale structures, or high catalytic activity, aiding in polysulfide adsorption and enhanced redox kinetics[38]. On the anode side, materials with uniform microstructure and low lithium adsorption energy help reduce side reactions, redistribute metal ion flow, and suppress dendrite growth.

(ii) The single-sided loading strategy focuses on bifunctional materials with both sulfiphilic and lithiophilic/sodiophilic properties. The bifunctional materials have high polarity and strong interactions with polysulfides and metal ions, significantly contributing to suppressing the shuttle effect and dendrite growth simultaneously. Compared to double-sided modifications, single-sided bifunctional materials are more cost-effective and help increase energy density while barely bringing additive weight to batteries.

Integrated strategies

Separator modification alone cannot fully address the slow redox kinetics, volume changes, and side reactions in Li/Na-S batteries. Thus, integrated strategies that combine separator functionalization with electrode modification and electrolyte optimization are crucial[39]. Through the combined effects of modified cathodes and functionalized separators, ion transport and reaction kinetics between the separator and cathode are accelerated, leading to better capacity retention of the battery. With the combined effects of modified metal anodes and/or artificial SEI layers along with functionalized separators, the flux of metal ions is maximally regulated, resulting in uniform metal deposition and the suppression of dendrite growth.

Furthermore, the synergistic effects of optimized electrolytes and functionalized separators enhance the transport of electrons and ions, accelerate solid-liquid and liquid-phase reactions, and suppress side reactions[40]. Despite being constrained by cost and production conditions, integrated strategies remain a vital approach to maximizing the capacity, energy density, cycle life, and safety of metal-sulfur batteries.

Requirements for functional separators

The inherent drawbacks of the sulfur cathode and Li/Na anode impose specific requirements on functionalized separators of Li/Na-S batteries[41]. Due to the shared pursuit of high energy density, high power, and long cycle life, the functionalized separators for Li-S and Na-S batteries exhibit similar requirements. However, due to superior high-power discharge, fast-charging performance, and higher cost-effectiveness, Na-S batteries demonstrate advantages over Li-S batteries in high-power and large-scale energy storage systems. Therefore, the design of functionalized separators for Na-S batteries should place additional emphasis on enhancing thermal stability, controlling polysulfides during high-current discharge, and regulating Na^+ flux.

Inhibiting the shuttle effect of polysulfide

Physical/chemical adsorption and catalytic conversion are considered the most important functionalization strategies to suppress the polysulfide shuttle and protect both sulfur and metal electrodes, as shown in Figure 2A[41], which enhance the adsorption capacity for polysulfides, confining polysulfides to the cathode side of the separator and accelerating the conversion rate of polysulfides. Unlike in Li-S batteries, where Li_2S is the only thermodynamically stable species after full discharge, Na_nS (with n = 1, 2, 4, 5) in Na-S batteries exhibits significant thermodynamic stability at room temperature, which may precipitate out of the electrolyte as solids during discharge. Therefore, for separators in Na-S batteries targeting the inhibition of the shuttle effect, simultaneously blocking and regulating the shuttle and precipitation behavior of polysulfides presents a new challenge and a critical requirement.

(a) Physical blocking

Physical blocking against polysulfides generally relies on electrostatic repulsion and sieving effects to achieve physical and spatial confinement of polysulfides, as shown in Figure 2B[42]. Firstly, according to the electrostatic repulsion principle, introducing negative charges on the separator is favorable for confining S_n^{2-} and $S_{n/2}^-$ species after ionization and dissociation to the cathode side and preventing soluble M_2S_n ($4 \leq n \leq 8$) from migrating across the separator. However, the accumulation of negatively charged polysulfides around the cathode can lead to the formation of a low-conductivity inert layer on the cathode surface and hinder metal ion plating. Therefore, it is essential to precisely regulate the charge density of the separator. The sieving effect strategy aims at constructing elective free transport of Li^+/Na^+ by utilizing the particle size difference between polysulfides and alkali metal ions. The diameter of Lithium and Sodium ions are only 1.52 and 2.04 Å, respectively, whereas the van der Waals diameters of higher-order polysulfides range from 10.99 to 19.19 Å which increase further when dissolved in the electrolyte[43]. Thus, constructing artificial small-sized nanopores on commercial separators (pore sizes of 50-100 nm for PP and 1.2-2.7 μm for cellulose separators) is a reasonable strategy to isolate larger polysulfides on the cathode side while allowing the free transport of Li^+/Na^+.

(b) Chemical adsorption

Chemical adsorption primarily relies on Lewis acid-base interaction and polar bonding adsorption to anchor the polysulfides and prevent the migration of soluble M_2S_n, as shown in Figure 2C[44]. Incorporating

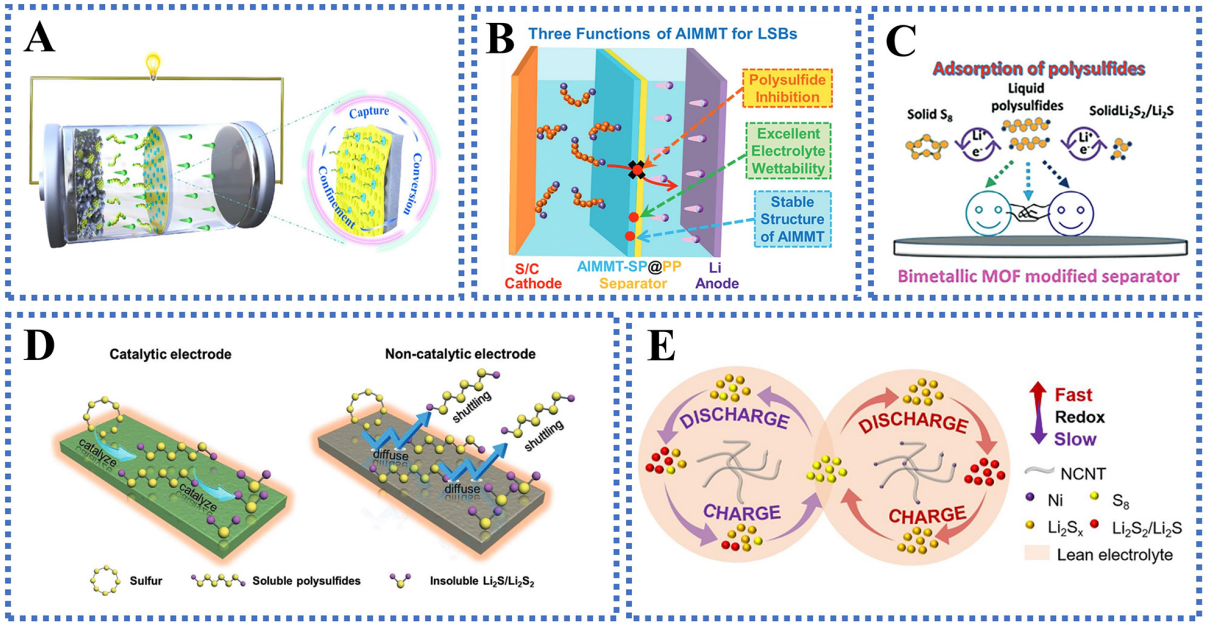

Figure 2. Requirements for inhibiting polysulfide shuttle effect. (A) Configuration diagram of a Li-S battery with a multifunctional separator. (B) Schematic illustration of physical blocking of polysulfides. (C) Schematic illustration of chemical adsorption of polysulfides. (D) Catalytic process of sulfur species conversions. (E) Illustration of the catalysis mechanism of Ni nanoparticles to polysulfides. This figure is quoted with permission from Yang *et al.*[41], Wang *et al.*[42], Razaq *et al.*[44], He *et al.*[47], and Zhang *et al.*[48], respectively.

materials with Lewis acid centers that accept electron pairs on the separator can improve the formation of coordinate covalent bonds with soluble polysulfides that donate electron pairs in electrolytes, thereby inhibiting the shuttle effect. As for polar bonding adsorption, the rich polar covalent bonds between sulfur atoms of different valence states in polysulfides make it feasible for polar materials to generate strong chemical interactions with polysulfides[45]. Thus, applying sulfiphilic polar materials is a promising choice for anchoring polysulfides through chemical adsorption and inhibiting the shuttle effect.

(c) Catalytic conversion

Enhancing the reutilization of adsorbed high-order sulfur species is critical to inhibiting the polysulfide shuttle effect. Once adsorbed, the polysulfide diffusion towards the anode is blocked, and the surface of the separator becomes the new platform for subsequent redox conversions instead of the anode. The separator interface becomes crucial for phase conversions of sulfur species and the return of converted polysulfides to the cathode[46]. Loading sulfiphilic catalytic materials or combining them with conductive substrates on the separator can accelerate redox kinetics, improve sulfur utilization, and enhance battery capacity retention, as shown in Figure 2D and E[47,48].

Suppressing dendrite growth

To inhibit the uncontrollable growth of lithium and sodium metal dendrites, strong lithiophilic/sodiophilic properties and uniform high-flux metal flow handling capabilities to regulate metal deposition behavior are crucial for functionalized separators in Li-S and Na-S batteries. Assisting in the formation of a stable and uniform SEI layer is also a key requirement for functionalized separators, especially for Na-S batteries.

Firstly, the separator is supposed to possess sufficient mechanical strength and puncture resistance so as to physically smash the dendrites before the penetration, as shown in Figure 3A[24,49]. Besides, the anode volume changes due to metal ions stripping/plating and the formation and breakdown of the SEI, and the transport of active substances will exert physical stress on the separator. Thus, enhancing physical strength is feasible to reduce the puncture risk caused by continuous dendrite growth.

Secondly, the uneven flow of metal particles is one of the major causes of lithium dendrite growth. Traditional separators with irregular pore sizes and poor electrolyte wettability lead to uneven ion deposition. Incorporating lithiophilic materials can create uniform, high-speed ion transport pathways, regulating ion migration and suppressing early-stage dendrite growth [Figure 3B][50,51].

Thirdly, facilitating the formation of a stable SEI layer on the anode surface is also a crucial function of the functionalized separator for suppressing lithium dendrite growth. The accumulated polysulfides on the anode not only disrupt the initially smooth plating/stripping anode surface but also form vulnerable SEI layers with a poor mechanical property that triggers continuous side reactions, metal and electrolyte consumption, and deteriorate the transport kinetics of metal ions, producing "dead Li/Na" and expediting dendrite growth, ultimately resulting in pulverization of the anode. Note that compared to lithium dendrites, sodium dendrites are relatively softer due to the lower Young's modulus of Na metal and conduct less pressure on the SEI layer. However, the SEI layer on the sodium anode is highly unstable, which exposes additional sodium nucleation sites after fracturing and exacerbates Na dendrite growth, leading to severe volume changes and internal stress compression on the anode. Therefore, functional separators are supposed to assist in forming a homogeneous structure and enhancing metal ion transfer capability to construct stable SEI layers with high ionic conductivity.

Bifunctional separators

In addition to addressing the shuttle effect, the strong influence of uncontrollable dendrite growth on the retention of capacity and cycling stability in Li-S and Na-S batteries makes it extremely important to explore bifunctional separators. Note that in this review, "monofunctional separators" refer to separators that have been specifically tested for the ability to block polysulfides, while "bifunctional separators" specifically refer to the separators that can simultaneously inhibit both the shuttle effect and dendrite growth.

The necessary capabilities of bifunctional separators are as follows [Figure 3C-E][52-54]: (i) Adequate mechanical intensity to withstand external pressure, mitigate interface issues, and counteract volume changes and dendrite growth; (ii) Appropriate physical/chemical polysulfide anchoring ability to inhibit the shuttle effect; (iii) Improved catalytic capability to enhance polysulfide conversion and utilization efficiency; (iv) Superior electrolyte wettability and suitable ionic and electronic conductivity for fast material transport; and (v) Enhanced metal ion adsorption and transport capabilities to regulate metal ion transport behavior and help for constructing stable SEI layers to achieve uniform metal ion deposition and prolonged cycling stability.

FUNCTIONALIZED SEPARATORS FOR LI-S BATTERIES

In recent years, the functionalization of separators of Li-S batteries has evolved from focusing solely on unifunctional separators that inhibit the polysulfide shuttle effect to establishing bifunctional separators that also suppress dendrite growth additionally and evolved from using double-sided modifications to address both issues separately to developing bifunctional materials that both sulfiphilic and lithiophilic.

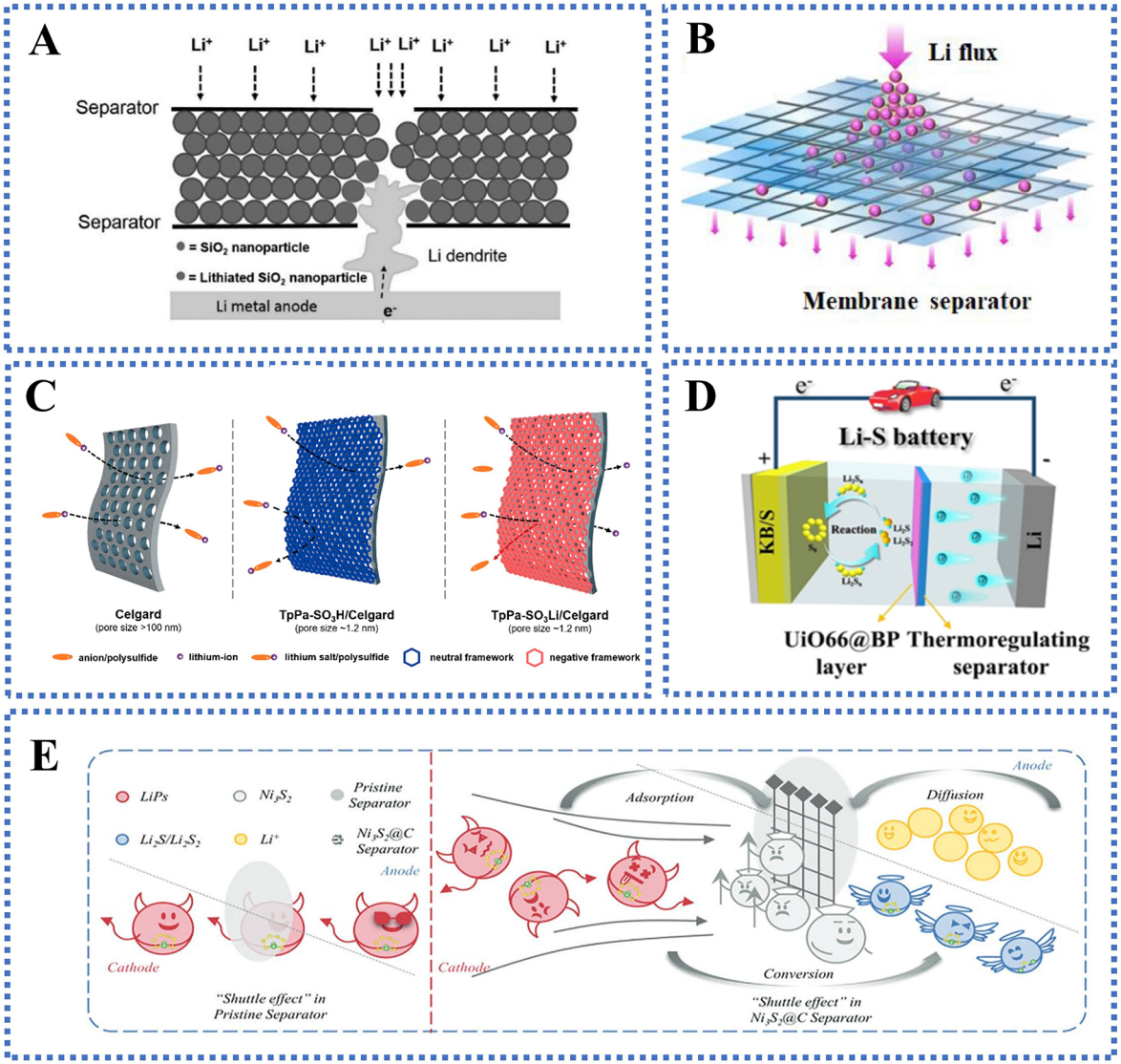

Figure 3. Requirements for suppressing metal dendrite growth and bifunctional separators. (A) Schematic illustration of strengthened separator countering dendrite growth. (B) Illustration of uniform lithium-ion transform. (C) Schematic illustration of lithium-ion conduction behavior in the functional separator. (D) Configuration of Li-S batteries with bifunctional separator. (E) Schematic of the working mechanism of bifunctional Ni_3S_2@C separator. This figure is quoted with permission from Liu *et al.*[24], Hou *et al.*[50], Cao *et al.*[52], Huang *et al.*[53], and Zhang *et al.*[54], respectively.

Monofunctional separators to inhibit shuttle effect

For the polysulfide shuttle effect inhibition, separator modification is primarily achieved through functional materials with physical properties such as electrostatic repulsion and nanoscale sieving capability, as well as chemical properties such as adsorption and catalysis.

Physical/chemical blocking and adsorption of polysulfide

Monofunctional interlayers for suppressing shuttle effect are generally categorized into: carbon materials with excellent mechanical properties and diverse microstructures, metal-organic frameworks (MOFs)/covalent organic frameworks (COFs) and polymers with tunable microstructures and functionalization feasibility, and polar metal compounds.

(a) Carbon materials

Carbon nanomaterials encompass diverse interesting nanostructures, including 0D dots, 1D nanowires and nanotubes, 2D nanosheets, and 3D nanospheres and foam networks. Certain carbon nanomaterials, such as graphene and carbon nanotubes (CNTs), exhibit excellent conductivity that can accelerate electron and ion transport and facilitate the formation of electrostatic/chemical adsorption networks for polysulfides, thereby suppressing the shuttle effect and enhancing the utilization of the sulfur cathode[55].

Liu *et al.* introduced a thin carbon layer derived from cathode inert materials into the separator, which utilized existing cathode materials and avoided additional weight, as shown in Figure 4A[56]. Carbon materials enriched with heteroatoms such as N, O, and B play a significant role in the chemical adsorption of polar polysulfides[57,58]. A biomass carbon doped with nitrogen and oxygen is endowed with abundant micro/mesoporous structure, grand specific surface area, ideal electrical conductivity, and the nitrogen and oxygen heteroatoms that exhibit strong chemical adsorption for lithium polysulfides (LiPSs), which synergistically ensure adequate adsorption of polysulfides[59]. The carbon materials with rich porous structures can extend the diffusion path of polysulfides from the sulfur cathode to the metal anode and enhance the adsorption efficiency of incorporated functional materials. Ma *et al.* incorporated a 3D mesoporous carbon nanocage on PP as a polysulfide buffer and cathode redox conversion boosting layer which redistributes the sulfur species through the abundant mesoporous structure[60]. CNTs provide abundant deposition sites for LiPSs due to their outstanding electrical conductivity, superior mechanical strength and chemical stability and large specific surface area derived from the 1D novel nanostructure, and are widely used as one of the preferred materials for shuttle-effect-suppressing materials. The composite interlayer of mesoporous multi-walled CNTs and ferroelectric barium titanate with high dielectric constant can serve as a "conductive scaffold" in Li-S batteries, providing sufficient conductive pathways for ion and electron transport adsorption capacity for LiPSs[61]. Graphene is another commonly used 2D conductive carbon substrate. Jiang *et al.* demonstrated the effectiveness of directly using graphene oxide (GO) as a functional layer coated on PP, as shown in Figure 4B[62]. Reduced GO (rGO), with abundant electronegative functional groups, not only easily forms electrostatic composites with other materials but also effectively blocks polysulfides through electrostatic repulsion[63]. A thin layer of rGO and sodium lignosulfonate composite with a porous network structure directly coated on PP can achieve electrostatic repulsion polysulfides through the abundant negatively charged sulfonate groups in SL, while still allowing normal Li^+ ion transport[64].

(b) MOF and COF materials

MOF and COF materials possess adjustable porosity, large surface areas, and highly-ordered uniform porous structures that are typically smaller than the dimensions of higher-order LiPSs, enabling MOFs/COFs to block the liquid-phase diffusion of long-chain and large-size polysulfides by sieving effect[65]. Moreover, MOFs/COFs can not only serve as conductive substrates but also act as sacrificial templates and the MOFs can provide abundant Lewis acidic centers for strong interaction with soluble polysulfides[66]. A carbon photon crystal (CPC) with 3D ordered hierarchical porous structure can be synthesized by templating method, as shown in Figure 4C[67]. The CPC-modified separator leverages the hierarchical macro-meso-microporous network to act as a polysulfide trap and boost the adsorption of LiPSs and reutilization of active sulfur. Despite high surface area, tunable pore structures, and excellent thermal and chemical stability, MOF/COF materials face challenges due to the inherently fragile structures and complex synthesis processes. These factors can lead to degradation during cycling and increased costs, which are detrimental to large-scale commercial applications.

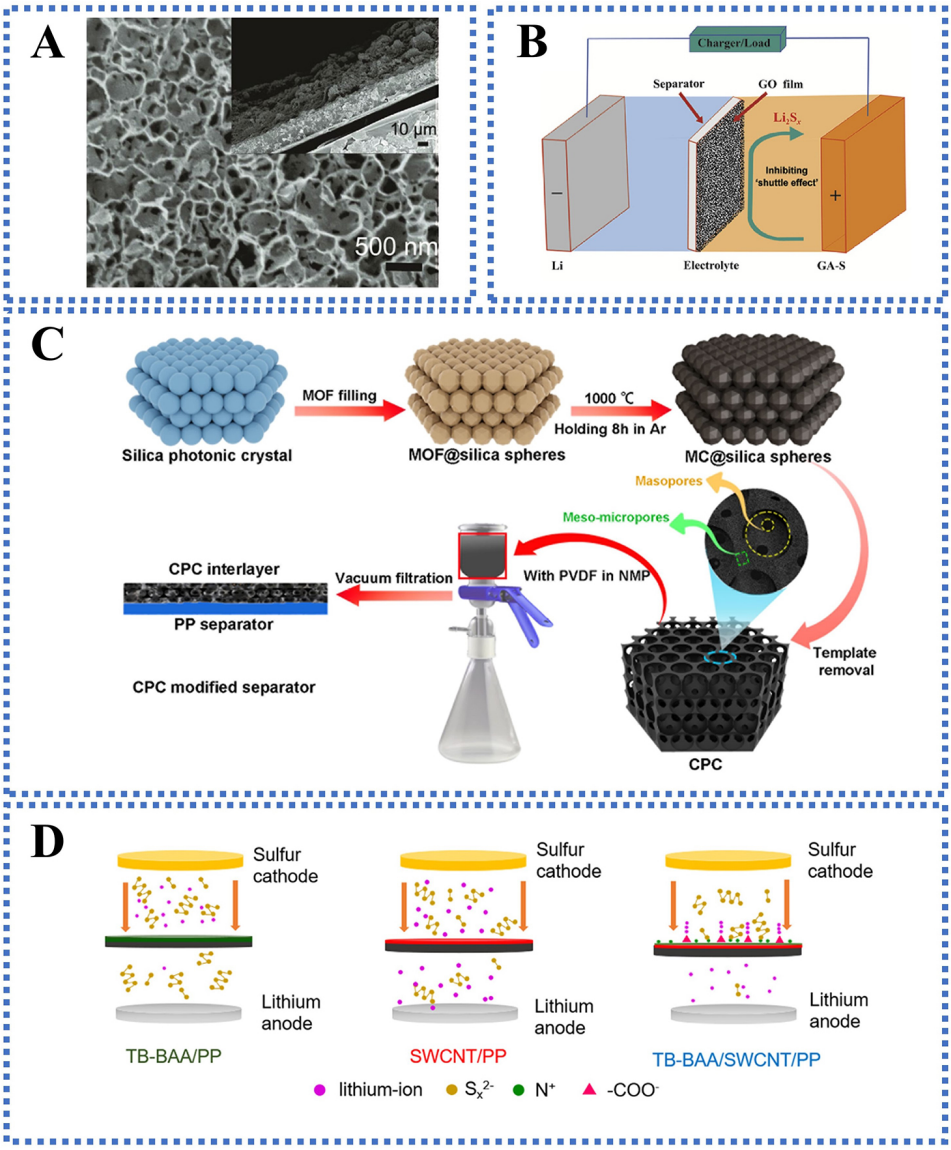

Figure 4. Monofunctional separators with carbon materials, MOF/COF and polymers for Li-S batteries. (A) SEM and TEM images of PCN. (B) Schematic of Li-S cells with GO-coated separator. (C) Fabrication process of batteries with CPC separators. (D) Schematic illustrations of Li-S cells with TB-BAA/SWCNT/PP separators. This figure is quoted with permission from Liu *et al.*[56], Jiang *et al.*[62], Zhang *et al.*[67], and Sun *et al.*[69], respectively.

(c) Polymers and polymer additives

The inherent complex microporous and mesoporous structures of polymers are highly beneficial for spatially inhibiting the diffusion of polysulfides. Conductive functionalization techniques can further enhance the chemical adsorption capacity of polymers for polysulfides[32]. Moreover, polymers possess a mature and controllable fabrication process, significantly reducing manufacturing costs and process complexity[68]. Sun *et al.* constructed a novel zwitterionic microporous polymer (TB-BAA) on the grooved layer of single-walled CNTs (SWCNTs) as presented in Figure 4D[69]. The ultra-thin TB-BAA top blocking layer, with zwitterionic groups, assisted in constructing constrained ion channels with lithiophilic and sulfiphilic groups, ensuring lithium-ion conductivity while simultaneously fixing polysulfides. The

SWCNTs provided ample electron transport channels, reduced and homogenized the pore size of the PP membrane, and minimized the penetration of TB-BAA.

In short, inherent insulative polymers are unfavorable for enhancing the conversion efficiency of LiPSs and the redox kinetics of sulfur cathodes, making the efficiency of LiPSs blockage ability inferior to that of carbon or MOF/COF-based composites. However, the low-cost, controllable microstructure construction techniques make the development of polymer additives and polymer-based composite materials highly competitive.

(d) Common Metallic Compounds

Common metals, except for transition metals, can provide a certain degree of mechanical strength to serve as physical barriers against LiPSs and can form polar chemical bonds with non-metal elements, which enables the LiPSs immobilization of common metallic compounds[70]. Aluminum oxides exhibit good mechanical strength and thermal conductivity and are favorable for heat redistribution during battery cycling[71]. Lin *et al.* developed an interlayer based on a mesoporous alumina and graphene (MA@G) composite in Figure 5A[72]. The mesoporous structure and high specific surface area (598 $m^2 g^{-1}$) of MA provide abundant exposed adsorption sites for LiPSs and have a low migration barrier for lithium, facilitating the suppression of LiPSs and the rapid transport of lithium[72]. Some metal compounds can form nanosheets or other particular morphologies through self-assembly or liquid exfoliation, achieving larger specific surface areas and more exposed adsorption sites for LiPSs. Zhang *et al.* utilized ultrasonically exfoliated MgB_2 nanosheets on the surface of PP, providing d increased specific surface area and pore volume and the ability to accommodate the volume expansion associated with the conversion of lithium sulfide (Li_2S) as shown in Figure 5B[73]. Unfortunately, due to the limited catalytic ability in the subsequent processes after immobilizing LiPSs, the application of common metal compounds in functionalized separators for Li-S batteries is significantly restricted.

Catalytic conversion of polysulfide

After being captured, the LiPSs are confined to the cathode side of the functional separator and participate in the subsequent conversion reactions ($S_8 \rightleftarrows Li_2S$)[74]. Therefore, the catalytic capability of the separator exerts significant impact on the conversion and reutilization efficiency of LiPSs that crucial for enhancing the redox reaction rate and utilization efficiency of the sulfur cathode. The catalytic functionalization of the separator in Li-S batteries primarily relies on transition metal compounds (TMCs) and the composites. Transition metals, located in the d-block and ds-block of the periodic table, can provide lone pair d-orbital electrons to act as nucleophiles or offer unfilled d-orbitals to act as electrophiles in chemical reactions, demonstrating strong catalytic activity. Moreover, the TMCs also exhibit strong redox properties but possess more stable chemical and thermodynamic characteristics, which is beneficial for reducing the activation energy of LiPSs conversion reactions and facilitating the rapid formation of intermediate LiPSs products[75]. Additionally, TMCs can be easily synthesized into novel microstructures such as quantum dots and nanoribbons by simple chemical methods that further enhance the adsorption and catalytic capabilities of LiPSs[76].

In transition metal oxides, the metal-O polar chemical bonds in transition metal oxides exhibit strong reactivity with polar LiPSs, providing abundant deposition sites for LiPSs, and demonstrate impressive catalytic activity, promoting the chemical adsorption and catalytic conversion of LiPSs[77]. The acrylic cloth carbon (ACC)/MnO_2 hybrid material synthesized via hydrothermal method by Zuo *et al.* can serve as an efficient LiPSs captor and catalyst. The ACC substrate in ACC/MnO_2 provides a broad conductive network

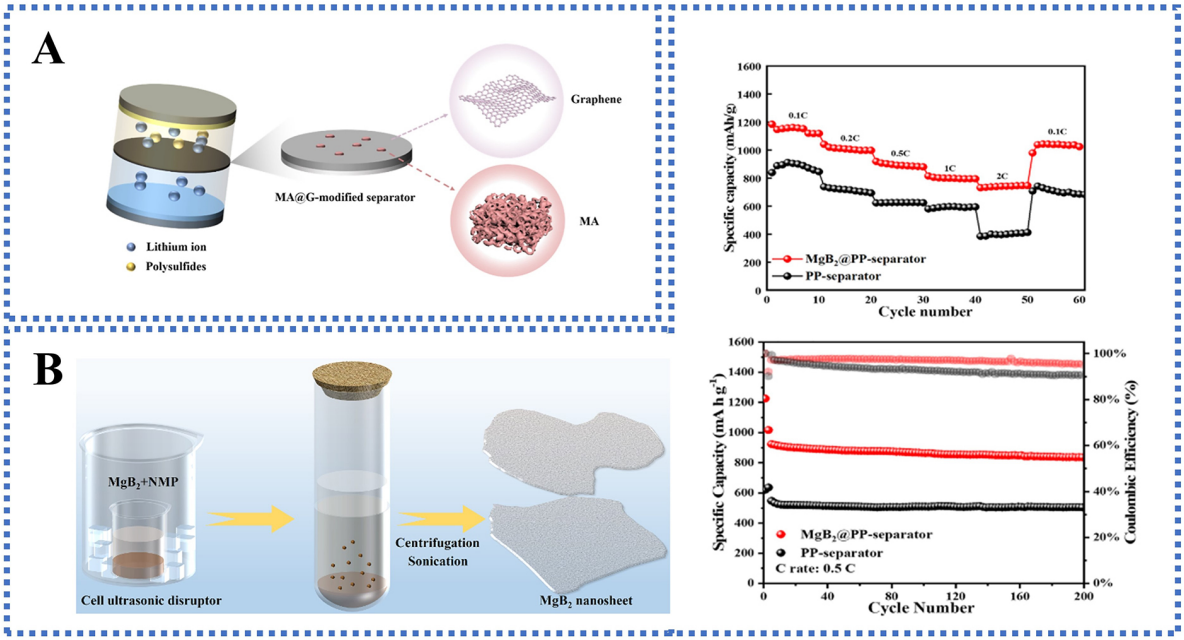

Figure 5. Functional separators with common metal compounds for Li-S batteries. (A) MA-Based Interlayer. (B) Peeling process of MgB_2, rate performance and cycle performance at 0.5C of the cell using MgB_2@PP separator. This figure is quoted with permission from Lin *et al.*[72], and Zhang *et al.*[73], respectively.

for electron and Li^+ transport, while the polar MnO_2 offers strong chemical affinity for LiPSs and exhibits superior redox kinetics [Figure 6A][78]. Zhu *et al.* fabricated coated separators with CeO_2 nanoparticles supported on multi-walled CNTs (MWCNTs/CeO_2/PP), as shown in Figure 6B[79]. The high affinity of CeO_2 for polysulfides effectively prevents the LiPSs transport through the separator, while the MWCNTs block polysulfide shuttling through physical adsorption and act as secondary current collectors to facilitate charge transfer[79]. Compared to oxides, transition metal sulfides, phosphides and selenides have greater atomic numbers and can form stronger polar chemical bonds with metals, resulting in enhanced polysulfide adsorption capabilities[80]. The interlayer with aligned hollow Co_9S_8@MOF arrays grown *in situ* on Celgard separators developed by He *et al.* helps to block LiPSs shuttling and fully utilize the sulfur cathode, which exhibits excellent long-cycle stability even under high sulfur loading of 5.6 mg cm^{-2} [Figure 6C][81]. The MoS_2 nanosheet/PP composite separator obtained through a simple exfoliation method features strong polarity from MoS_2 that enables effective adsorption and anchoring of polysulfides as in Figure 6D. Besides, the large specific surface area of the nanosheet structure provides abundant Li^+ adsorption sites and guarantees rapid adsorption and transport of Li^+[82]. Fan *et al.* designed a coral-like porous composite functional layer containing molybdenum disulfide (rGO/MoS_2/C) with large specific surface area and good electrolyte wettability[83]. The active sites of MoS_2 effectively enhance the adsorption of LiPSs, demonstrating excellent cycling stability with a capacity decay of only 0.022% per cycle after 1,000 cycles at 2.0C. The symmetric cell with the rGO/MoS_2/C composite showed a larger CV curve enclosed area, indicating a lower energy barrier for the catalytic conversion of Li_2S_n[83]. Zhou *et al.* prepared a novel interlayer composed of Fe_3Se_4/FeSe heterojunctions encapsulated by two-dimensional (2D) MXene nanosheets through the *in situ* growth and selenization of Fe-MOFs[84]. The Fe_3Se_4/FeSe@MXene interlayer exhibits low adsorption energies on the surfaces of S_8, Li_2S_8, Li_2S_6, Li_2S_4, Li_2S_2, and Li_2S owing to the MXene framework and the outstanding synergistic catalytic effect of the Fe_3Se_4/FeSe heterojunctions[84]. Wang *et al.* employed continuous low-temperature chemical vapor deposition to controllably grow generic graphene-$MoSe_2$ heterostructures (Gr-M_xSe_y) on commercial GF separators[85]. The coupling of graphene with $MoSe_2$ as a polar and catalytic

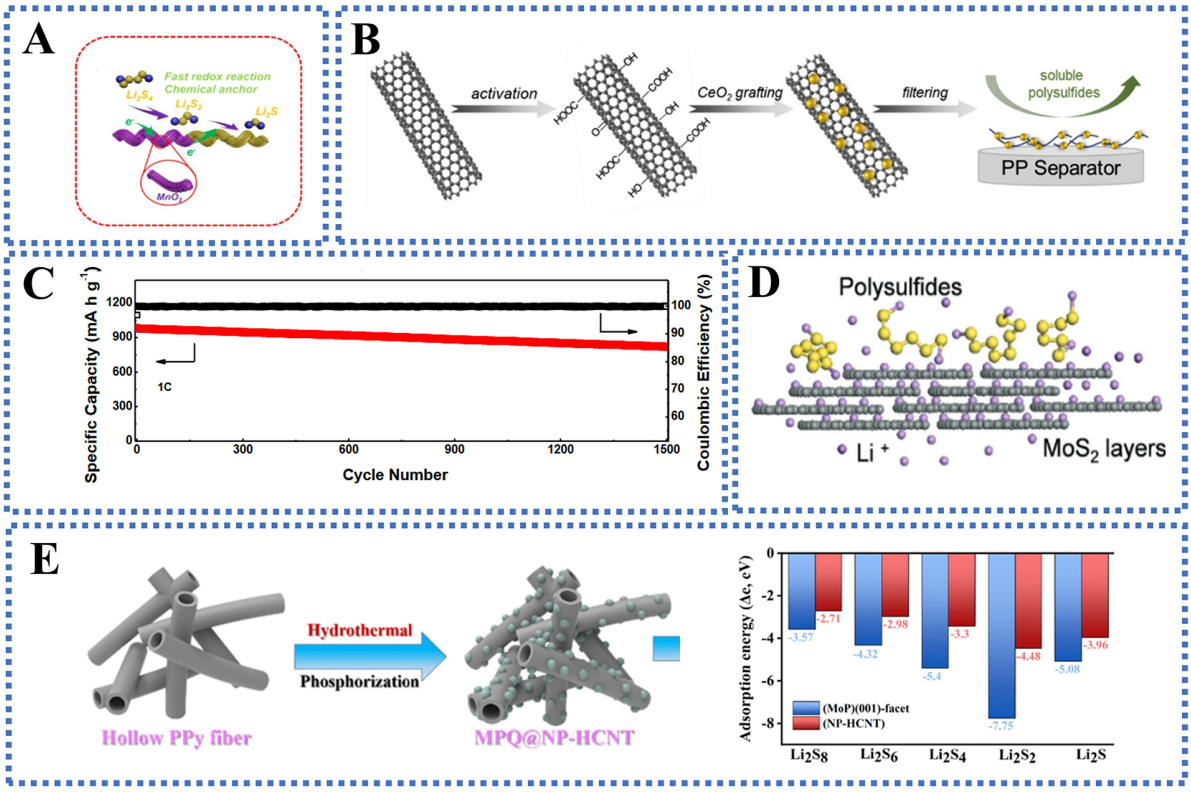

Figure 6. Functional separators with transition metal compounds for Li-S batteries. (A) LiPSs adsorption and catalytic effect of ACC/MnO_2. (B) Preparation of PP-MWCNTs/CeO_2 separators. (C) Long-term cycling profile at 1C of the Li-S cells with the Co_9S_8 coated separators. (D) Schematic of LiPSs adsorption of MoS_2/Celgard separator. (E) Fabrication and adsorption energies of the MPQ@NP-HCNT. This figure is quoted with permission from Zuo *et al.*[78], Zhu *et al.*[79], He *et al.*[81], Ghazi *et al.*[82], and Zhang *et al.*[86], respectively.

framework creates hybrid energy levels, enhancing the conductivity and electrocatalytic activity of the separator for sulfur redox reactions. The Gr-M_xSe_y/GF separator demonstrated high capacities of 1,118.7 mAh g^{-1} at 0.2C and 552.8 mAh g^{-1} at 3C[85]. Unique structures such as quantum dots aid in the uniform and dense distribution of TMCs on the separator surface, enabling functionalization with less mass and higher chemical activity. The MoP quantum dots@N, P-doped hollow polypyrrole interlayer utilizes the excellent chemical adsorption and catalytic conversion capabilities of MoP quantum dots to suppress the LiPS shuttle effect [Figure 6E][86].

C, N, and B atoms have more diverse valence states than O, resulting in stronger polar metal-C/N/B bonds and higher chemical stability[87]. Transition metal carbides, nitrides (TMNs), and borides (TMBs) have relatively low average molecular masses, which hardly bring additional mass to the batteries. Compared to metal-O bonds, LiPSs are more inclined to bond with the stronger polar metal-C/N/B bonds, leading to lower adsorption and conversion energy barriers for LiPSs. Moreover, transition metal carbides, TMNs, and TMBs can easily achieve structural regulation by controlling synthesis conditions, resulting in microstructures such as nanowires and quantum dots that provide abundant anchoring sites for LiPSs and adsorption sites for Li^+. The Mo_2C/C can act as a polar catalytic interlayer and exhibit dynamic adsorption and promoted kinetics for the reversible conversion of LiPSs[88]. According to Pan *et al.*; the polar Fe_3C and doped N in Fe_3C-N-doped rGO enhanced atomic attraction for sulfur and LiPSs and achieved higher capacities at increased current densities as in Figure 7A[89]. Ma *et al.* designed and synthesized a novel

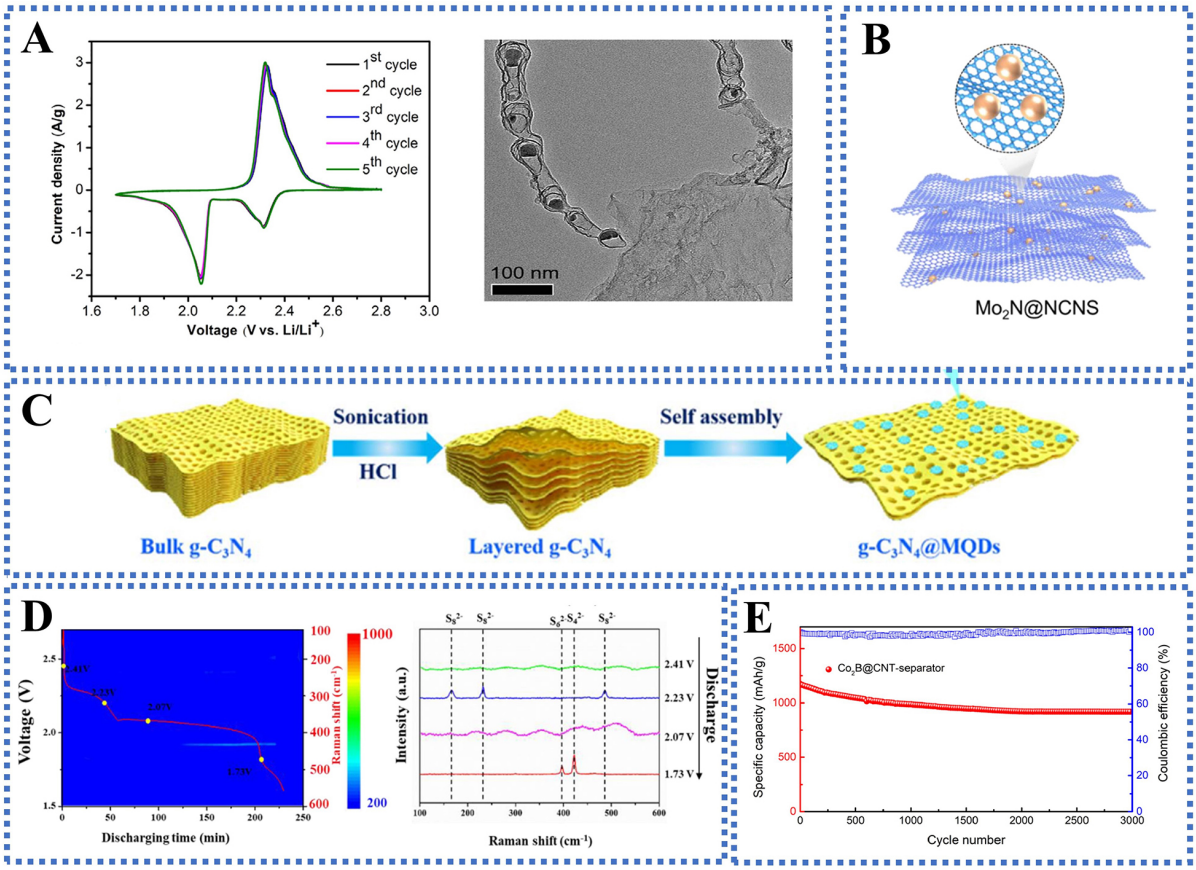

Figure 7. Functional separators with catalytic transition metal compounds for shuttle effect inhibition. (A) Cyclic-voltammetry profiles of Fe_3C-N-rGO coated separator and TEM image of Fe_3C-N-rGO. (B) Schematic illustration of Mo_2N@NCNS. (C) Preparation schematic diagram of g-C_3N_4@MQDs. (D) *In situ* Raman spectra in discharging processes of the cells with TiB_2/PP separators. (E) Long life cycle performance and Coulombic efficiency at 5C Li-S cells with Co_2B@CNT-separator. This figure is quoted with permission from Pan *et al.*[89], Ma *et al.*[91], Yang *et al.*[41], Li *et al.*[93], and Guan *et al.*[94], respectively.

nitrogen-doped graphene (NG) nanosheets embedded with conductive $WN_{0.67}$ nanoneedle that enable rapid electron/ion transfer, effective anchoring of LiPSs, promotion of uniform Li_2S nucleation/growth, and improved sulfur utilization[90]. As exhibited in Figure 7B, monodispersed Mo_2N quantum dot-modified nitrogen-doped carbon nanosheets (Mo_2N@NCNS) have also been proven to be an effective interlayer. The Mo_2N quantum dot enhances the intrinsic conductivity of the 3D NCNS network and provides abundant catalytic sites and strong polarity. Mo_2N@NCNS not only regulates the random motion of LiPSs through physical confinement and chemical adsorption, but also exhibits superior LiPSs catalytic and promotes the nucleation and deposition of Li_2S_2/Li_2S, thereby enhancing the overall electrochemical performance of Li-S batteries[91]. Two-dimensional transition metal carbides, TMNs, or carbonitrides (MXenes) also exhibit surprising adsorption and catalytic capabilities for LiPSs due to the regular 2D sheet structure, large specific surface area, and abundant polar deposition sites[92]. As shown in Figure 7C, Yang *et al.* addressed the agglomeration issue by using the electrostatic adsorption principle to self-assemble MXene quantum dots (MQDs) on the surface of g-C_3N_4 sheets to provide more active sites for capturing dissolved LiPSs[41].

Compared to carbides and nitrides, borides are more abundant on Earth and contribute to more economical separator functionalization. The TiB_2, with a gradient distribution of conductive sites, adsorbs polysulfides via polar chemical bonds and accelerates the conversion by high catalytic properties as shown

in Figure 7D[93]. The Co_2B@CNT layer on PP developed by Guan *et al.* exhibited a high polysulfide trapping capability (Li_2S_6 at 11.67 mg/m^2) owing to the co-adsorption of Co and B and showed a significant catalytic effect for the conversion of Li_2S_8 to Li_2S due to the catalytic Co [Figure 7E][94]. Due to the metalloid properties of boron and the abundant polysulfide adsorption sites, borides can form highly active planar-like polysulfide adsorption networks when uniformly dispersed on conductive substrates and exhibit excellent capabilities in suppressing the shuttle effect[51,95,96].

In conclusion, TMCs with unique morphologies, such as quantum dots, nanowires/needles/ribbons, and nanosheets, serve as superior anchoring site doners and catalysts for LiPSs. As displayed in Table 1, the combination of TMCs with CNT, rGO, and MOF/COF frameworks aids in enhancing the mechanical strength of the separator and facilitates the construction of uniform and efficient networks for the adsorption and catalysis of LiPSs.

Bifunctional separators to suppress shuttle effect and dendrite growth

Double-sided separators

As mentioned before, double-sided separators for Li-S batteries generally show asymmetric structures in order to deal with shuttle effect of polysulfides and growth of lithium dendrites separately[99]. Wang *et al.* coated Al_2O_3 particles on the anode side and sodium CMC on the other side of PE[38]. The gel-polymer-inorganic separator utilizes the "polysulfide-phobic" interface formed by the CMC layer and the mechanical strength of Al_2O_3 to inhibit the growth of polysulfides and dendrites on the respective sides of the separator, as shown in Figure 8A[38]. Chang *et al.* proposed a sandwich separator loaded with a composite thermal conductive layer (TCL) made of V_2O_5 microspheres and Al_2O_3 nanosheets[100]. The V_2O_5 on the cathode side not only combines with the LiPS catalytic layer (LCL) on the surface of the S cathode to catalyze the conversion of LiPSs but also collaborates with the Al_2O_3 nanosheets on the anode side to redistribute Li^+ flux and thermal energy. The Li-S batteries with the TCL/PP separator demonstrated excellent cycling stability, with a capacity decay rate of 0.036% per cycle over 2,000 cycles at a 1C rate as shown in Figure 8B[100]. Dang *et al.* grew continuous cerium-based metal-organic framework-808 (Ce-MOF-808) on both sides of the PP separator[101]. Due to the highly ordered nanostructure and polar groups, Ce-MOF-808 on the cathode side performs multiple functions of selective sieving, adsorption, and catalytic conversion of LiPSs. On the anode side, it promotes the rapid diffusion of Li^+ and facilitates stable nucleation and growth of lithium [Figure 8C][101].

Bifunctional interlayers on separators

Polar materials are one of the most common bifunctional materials and are generally combined with conductive substrates to further improve the surface structure of the pristine separator[102,103]. Wang *et al.* applied anodic aluminum oxide (AAO) interlayers with high rigidity and non-flammability to enhance the safety of Li-S batteries. The orderly microstructure of AAO facilitates rapid transport channels for Li^+, reducing the area-specific resistance and accelerating redox reactions[104]. Liu *et al.* embedded ZrO_2 nanoparticles into a polyetherimide (PZ)-based separator using interfacial polymerization to enhance the Li^+ transference number (0.55) and diffusion coefficient (2.16×10^{-8} cm^2 s^{-1}) of the ZrO_2/PZ separator[105]. The impressive bifunctionality of the ZrO_2/PZ is attributed to the pore size regulation, promoted electrostatic repulsion, and physical/chemical adsorption[105].

TMCs exhibit excellent sulfiphilic and lithiophilic properties owing to the rich d-orbital electronic states and polar chemical bonds, making them the ideal bifunctional materials for fabricating separator interlayers. The double-sided "nanobrick wall" structure constructed by layer-by-layer self-assembly of MoS_2 and poly(diallyldimethylammonium chloride) with poly(acrylic acid) (PAA), marked as $(M\text{-}P/P)_{10}$,

Table 1. Summary of electrochemical performance of Li-S batteries (coin cell) with monofunctional separators

Separators	Sulfur loading (mg cm^{-2})	Cycling performance	Ref.
HNPC/PP	4	930 mAh g^{-1} at 0.2C, 67.1% after 200 cycles	[58]
CBBC/PP	1.5~2.0	1,098.2 mAh g^{-1} at 0.5C, 59.7% after 200 cycles	[59]
PCN-PP	7.34	1,044 mAh g^{-1} at 1C, 62.45% after 200 cycles	[60]
CNTOH/PE	3	1,056 mAh g^{-1} at 0.5C, 53.4% after 400 cycles	[97]
rGO/PP	1.5	1,067 mAh g^{-1} at 0.2C, 82.3% after 100 cycles	[63]
rGO@SL/PP	1.5	707 mAh g^{-1} at 2C, 74% after 1,000 cycles	[64]
G-PSS+N,-G/separator	0.8	1,012 mAh g^{-1} at 1C, 74.1% after 700 cycles	[98]
CPC/PP	3	1,214 mAh g^{-1} at 1C, 50.5% after 1,500 cycles	[67]
TpPa-SO_3Li/ Celgard	5.4	≈600 mAh g^{-1} at 4C, 84.8% after 400 cycles	[52]
TB-BAA/ SWCNT/PP	3	946 mAh g^{-1} at 1C, 72.5% after 500 cycles	[69]
PAN@APP	1.8	601 mAh g^{-1} at 2C, 83.2% after 800 cycles	[4]
MA/G@PP	1	808 mAh g^{-1} at 0.5C, 57.1% after 100 cycles	[72]
MgB_2@PP	1.3	732 mAh g^{-1} at 2C, 67.8% after 500 cycles	[73]
ACC/MnO_2/PP	5	993 mAh g^{-1} at 0.2C, 71.7% after 300 cycles	[78]
Co_9S_8-Celgard	5.6	986 mAh g^{-1} at 1C, 83.2% after 1,500 cycles	[81]
rGO/MoS_2/C-Celgard	4.5	78% after 1,000 cycles at 1C	[83]
Fe_3Se_4/FeSe@MXene-PP	5.8	862.6 mAh g^{-1} at 0.2C, 92.3% after 120 cycles	[84]
MPQ@NP-HCNT-PP	1	937 mAh g^{-1} at 1C, 68.8% after 600 cycles	[86]
Fe_3C-N-GO /PP	0.7-1	774.8 mAh g^{-1} at 0.5C, 93.2% after 100 cycles	[89]
$WN_{0.67}$@NG/PP	1.2-1.5	71.2% after 800 cycles at 2C	[90]
Mo_2N@NCNS/PP	2	895 mAh g^{-1} at 2C, 76% after 800 cycles	[91]
g-C_3N_4@MQD -Celgard	1.2	486 mAh g^{-1} after 1,000 cycles at 2C	[41]
TiB_2/PP	2.88	823 mAh g^{-1} at 2C, 86% after 550 cycles	[93]
Co_2B@CNT /PP	3.8	1,172.8 mAh g^{-1} at 5C, 78.4% after 3,000 cycles	[94]

provides a high discharge capacity at a high 3C [Figure 9A][106]. Liu *et al.* prepared an ultra-small CoP (S-CoP, 25 nm) composite material embedded within CNT-modulated MOF. The S-CoP/CNT effectively promoted the conversion of Li_2S and provided ultra-long dendrite-free lithium deposition[107]. Li *et al.* designed an NbB_2/rGO modified PP separator (NbB_2/rGO/PP) and revealed that the catalysis of LiPSs by NbB_2 relies on the passivated surface with the oxide layer (O_2-NbB_2), where B-O-Li and Nb-O-Li bonds significantly lower the decomposition barrier of Li_2S[108]. The rapid conversion and reutilization of LiPSs help maintain the continuous exposure of active sites on the separator surface for Li^+ adsorption, which is beneficial for enhancing the lithium-ion diffusion rate as displayed in Figure 9B.

The TMCs with unique nanoscale microstructures can facilitate not only the highly effective entrapment of polysulfides but also the regular transport of Li^+, such as heterostructure TMCs with built-in electric fields and 2D layered TMCs with high specific surface areas[109]. Wang *et al.* designed a heterostructured MoP-MoO_2@defective porous carbon nanofibers (PCNFs) bifunctional interlayer with abundant anchoring sites as shown in Figure 10A[110]. Benefiting from the shortened Li^+ pathways provided by PCNFs, the heterostructured MoP-MoO_2 nanobelts exhibit excellent capabilities for intercepting and converting sulfur species and enabling long-term dendrite-free cycling of the anode[110]. As in Figure 10B, Lv *et al.* synthesized a unique VSe_2/V_2C heterostructure *in situ* by sacrificing a V_2C precursor, effectively combining the strong affinity of V_2C for LiPSs with the high electrocatalytic activity of VSe_2[111]. The local built-in electric field at the VSe_2/V_2C heterointerface significantly enhances electron and ion transport capabilities, ultimately improving the conversion kinetics of sulfur species and the transport kinetics of Li^+[111]. Incorporating MXene materials with high lithiophilicity and sulfiphilicity, derived from the inherent surface polar groups,

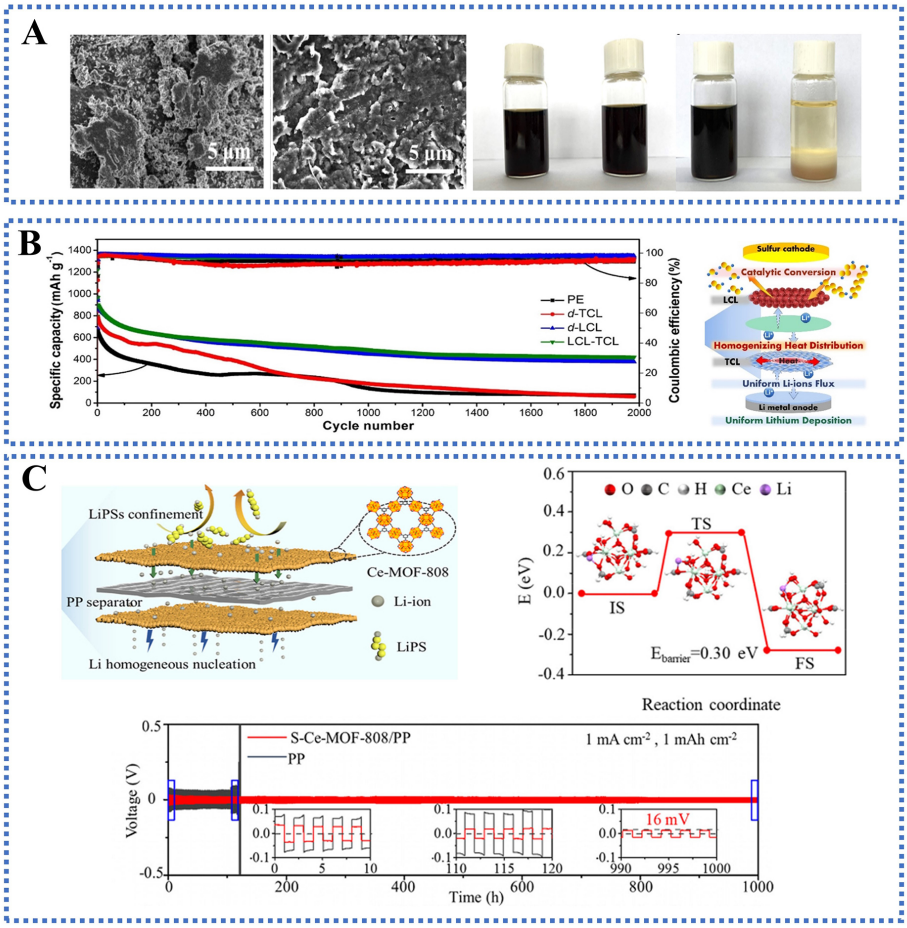

Figure 8. Double-sided bifunctional separators for Li-S batteries. (A) SEM images of the cycled Li-metal anodes disassembled from symmetrical cells with PP separator and the Al_2O_3-PE-CMC separator and polysulfide adsorption tests before and after adding CMC powder. (B) Long-term cycling performance of the LCL-TCL modified separator and the schematic of corresponding Li-S cells. (C) Configuration schematic of Li-S cells with Ce-MOF-808/PP separator, diffusion energy barrier of Li-ion of Ce-MOF-808, and the Li-Li symmetric cells voltage profiles. This figure is quoted with permission from Wang *et al.*[38], Chang *et al.*[100], and Dang *et al.*[101], respectively.

provides higher conductivity and optimal flexibility to the bifunctional interlayer, significantly accelerating the cross-separator transport of Li^+ and ensuring the integrity and stability of the Li-S batteries[112]. For the MXene covered with TiS_2/TiO_2 heterostructure on the surface (TOS/MX/TOS), the TiO_2 nanoparticles adsorb and inhibit LiPSs, while the high-conductive and catalytic TiS_2 nanoparticles significantly promote the conversion of long-chain LiPSs into short-chain Li_2S_2/Li_2S. The TOS/MX/TOS interlayer also protects the lithium anode by preventing the undesirable deposition of polysulfides on the anode surface and attains stable cycling performance, as shown in Figure 10C[113].

TMC quantum dots possess highly discrete electron and hole energy levels, resulting in more chemically active sites for the of polysulfide adsorption and Li^+ anchoring[114]. Dispersing TMCs on conductive substrates with high specific surface area ensures maximal uniform dispersion of the quantum dots, and facilitates comprehensive adsorption of LiPSs and further homogenizing Li^+ flux. Lithiophilic and sulfiphilic Mo_2N, Mo_2S, and VN quantum dots have been demonstrated to effectively suppress the shuttle effect and dendrite growth when modifying NG[115-117]. The porous NG framework serves as a 3D electronic channel

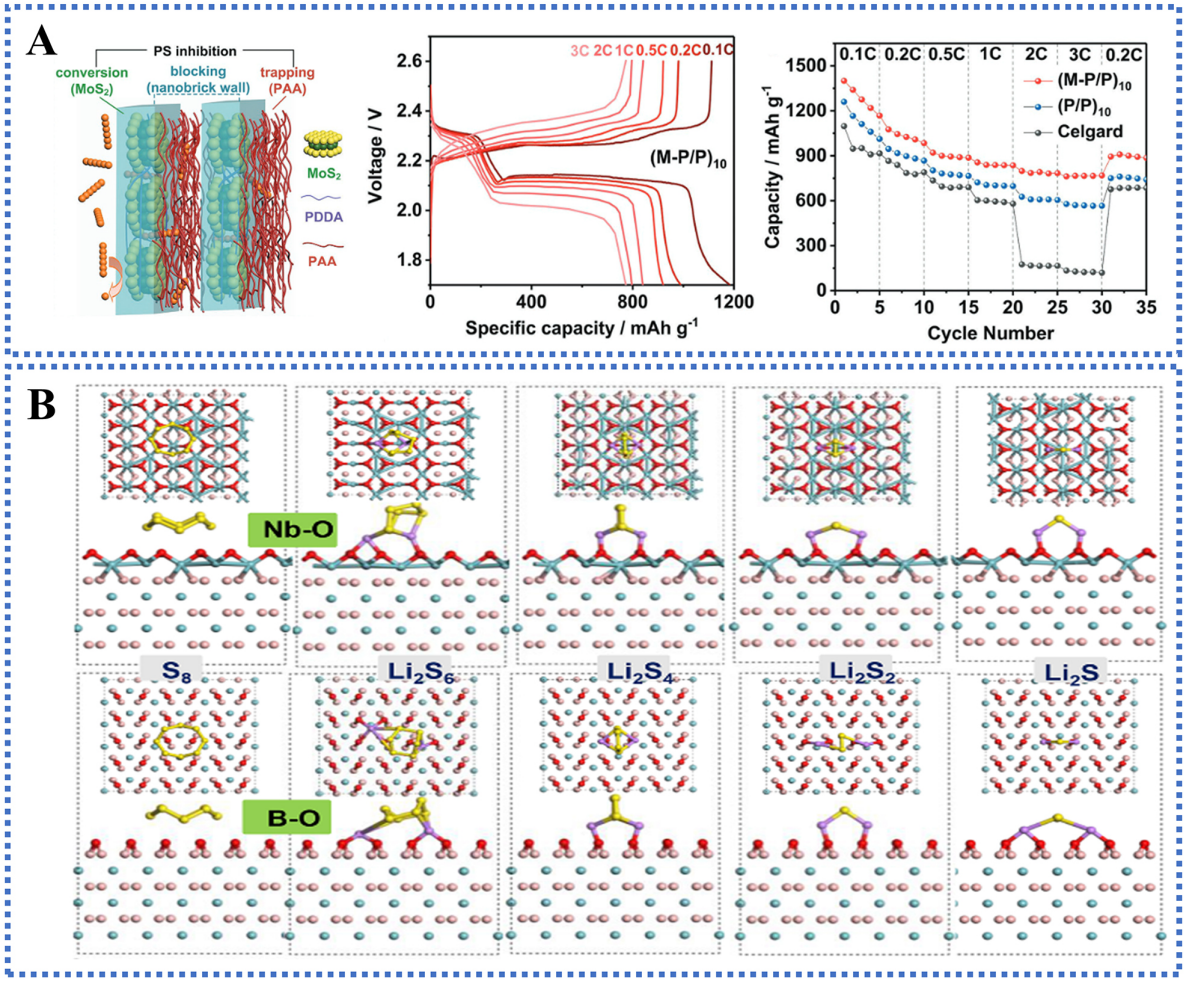

Figure 9. Bifunctional separators with polar TMBs for Li-S batteries. (A) Schematic diagrams, rate performance and charge-discharge curves of cells with M-P/P)$_{10}$. (B) Schematic of the LiPSs conversion on the NbB_2/rGO separator and adsorption configuration of Li_2S_n on O_2-NbB_2. This figure is quoted with permission from Wu *et al.*[106], and Li *et al.*[108], respectively.

and spatial reservoir for LiPSs adsorption, which not only physically confines sulfur species but also accelerates electron transfer during redox reactions and prolongs the nucleation time of lithium dendrites. Mo_2N quantum dots@NG exhibit higher Li^+ conductivity [Figure 11A] and excellent cycling stability at 2C[115]. In Figure 11B, Mo_2S quantum dots@nitrogen-doping reduced graphene oxides (NRGO), featuring abundant 10 nm mesopores and a high specific surface area of up to 69.18 $m^2 g^{-1}$, facilitates the full exposure of Mo_2S catalytic sites[116]. Mo_2S@NRGO possesses a lower Gibbs free energy (0.016 eV) and the free energy required for the decomposition of Li_2S^* (1.06 eV), which accelerate the liquid-solid conversion reaction from $Li_2S_4^*$ to $Li_2S_2^*$ and the solid-solid decomposition reaction of Li_2S, respectively. Similarly, VN quantum dots@NG, with a Li_2S dissociation energy barrier of only 0.31 eV on the VN (111) surface and the conductive network provided by the NG framework [Figure 11C], effectively achieve 1,000 h of dendrite-free stable cycling[117].

Furthermore, benefiting from the uniform pore sizes, MOF/COF materials can significantly contribute to the consistent Li^+ transport and preventing the formation of lithium dendrites[44,118,119]. The incorporation of polymer materials in functional separators can positively impact the electrolyte affinity of the separator and assist in the protection of the metal anode[120].

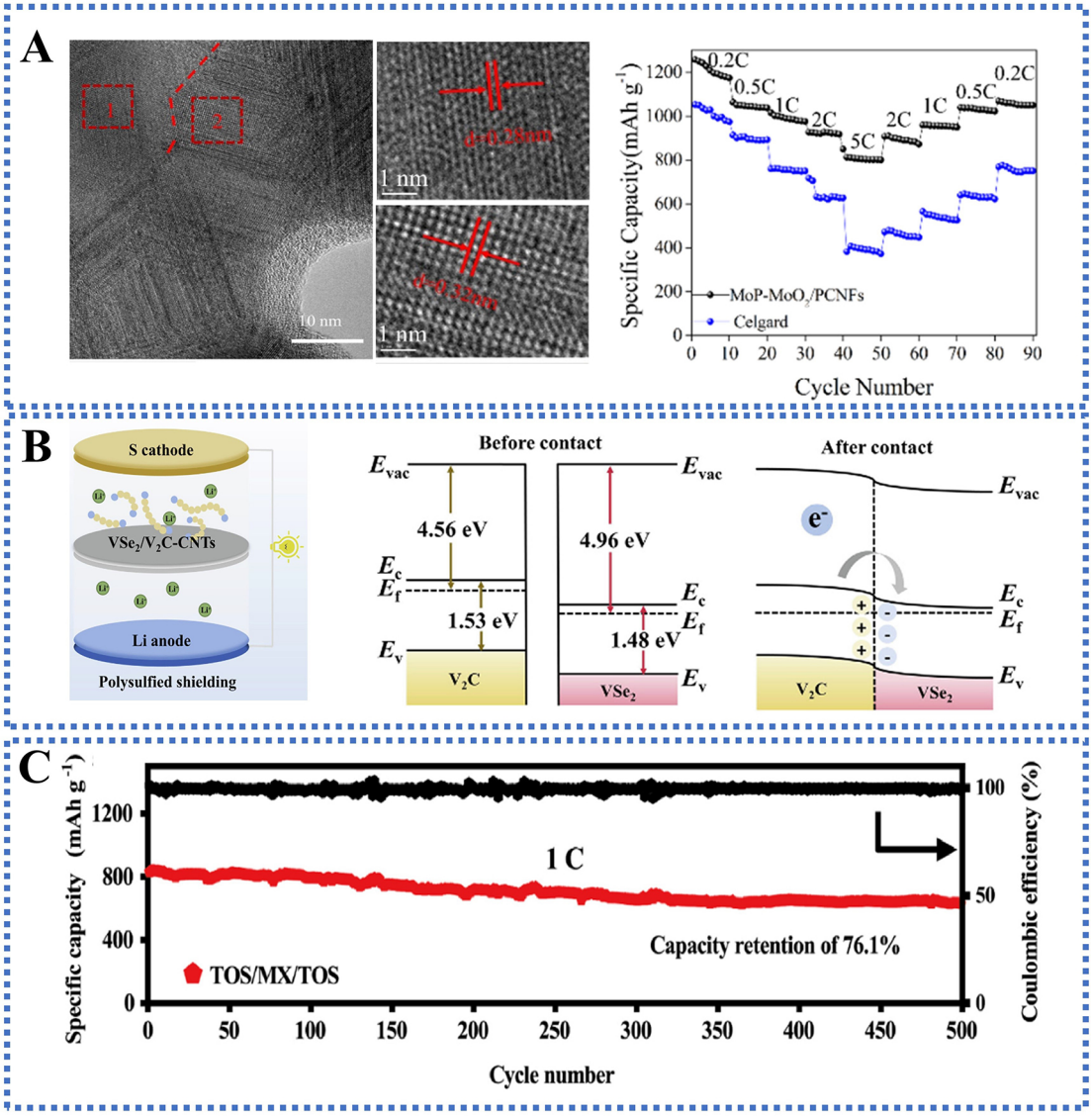

Figure 10. Bifunctional separators with MXenes and heterostructured TMBs for Li-S batteries. (A) HRTEM of MoP-MoO_2 and rate performance of the MoP-MoO_2/PCNT separator. (B) Schematic of Li-S cells with VSe_2/V_2C-CNTs-PP and energy band diagrams of V_2C and VSe_2. (C) Long-term cycling profile of the TOS/MX/TOS modified separator. This figure is quoted with permission from Wang *et al.*[110], Lv *et al.*[111], and Yao *et al.*[113], respectively.

According to the summary of performance of Li-S batteries with bifunctional separators in Table 2, compared to double-sided modification, bifunctional interlayers loaded with sulfiphilic and lithiophilic materials on a single-sided separator offer greater advantages in increasing cathode sulfur loading, enhancing the energy density and safety of Li-S batteries, simplifying the process, and reducing costs. This approach represents the main strategy for bifunctional separators in current Li-S battery technology.

Integrated strategies

Based on the functionalization of the separator, combining this approach with electrode optimization strategies can more effectively address the polysulfide shuttle effect on the cathode side and the growth of

Table 2. Summary of electrochemical performance of Li-S batteries (coin cell) with bifunctional separators

Separators	Cycling performance of Li//Li cell	Sulfur loading (mg cm^{-2})	Cycling performance of Li-S battery	Ref.
CTP-PAN-LLZTO	11.7 mV for 1,200 h at 2 mA cm^{-2}	3.5	1,287.9 mAh g^{-1} at 0.5C, 70.5% after 500 cycles	[99]
Al_2O_3-PE-CMC	55 mV for 400 h at 20 mA cm^{-2}, 4 mAh cm^{-2}	1	1,178.3 mAh g^{-1} at 0.5C, 60.95% after 500 cycles	[38]
Fe-ZIF-8/PP	36 mV for 1 h at 0.5 mA cm^{-2}	2.5~3.6	865 mAh g^{-1} at 0.5C, 47.3% after 1,000 cycles	[44]
Ce-MOF-808/PP	74 mV for 1,000 h at 1 mA cm^{-2}, 1 mAh cm^{-2}	5-7	954.7 mAh g^{-1} at 1C, 87.5% after 500 cycles	[101]
PPW/UiO66@BP	< 10 mV for 2,200 h at 0.5 mA cm^{-2}, 0.5 mAh cm^{-2}	4.76	1,157 mAh g^{-1} at 0.2C, 77% after 100 cycles	[53]
Ni_3S_2@C/PP	< 50 mV for 540 h at 10, 20, 50 mA cm^{-2}	4.52	1,048.5 mAh g^{-1} at 0.5C, 63% after 300 cycles	[121]
ZrO_2/PZ-PZ	< 20 mV for 500 h at 0.5 mA cm^{-2}, 0.5 mAh cm^{-2}	1	1,242 mAh g^{-1} at 0.2C, 68% after 200 cycles	[103]
$(M\text{-}P/P)_{10}$-Celgard	< 30 mV for 200 h at 1 mA cm^{-2}, 1 mAh cm^{-2}	1.2	1,007 mAh g^{-1} at 1C, 42% after 2,000 cycles	[106]
S-CoP/CNT-PP	< 50 mV for 1,714 h at 2 mA cm^{-2}, 2 mAh cm^{-2}	1.9	974.5 mAh g^{-1} at 0.5C, 59% after 500 cycles	[107]
VSe_2/V_2C-CNTs-PP	< 20 mV for 300 h at 1 mA cm^{-2}, 1 mAh cm^{-2}	1	1,001.3 mAh g^{-1} at 2C, 42% after 600 cycles	[111]
HE-MXene/G@PP	< 50 mV for 6,000 h at 40 mA cm^{-2}, 40 mAh cm^{-2}	6.5	> 500 mAh g^{-1} at 1C, 85.7% after 500 cycles	[112]
TOS/MX/TOS	75 mV for 1,000 h at 5 mA cm^{-2}, 5 mAh cm^{-2}	N/A	831.9 mAh g^{-1} at 1C, 76.1% after 500 cycles	[113]
NbN@NG/PP	< 50 mV over 1,000 h at 5 mA cm^{-2}, 1 mAh cm^{-2}	1.3-1.6	1,107 mAh g^{-1} at 0.2C, 86.4 % after 200 cycles	[114]
Mo_2N QDs@NG/PP	142 mV for 1,400 h at 5 mA cm^{-2}, 0.5 mAh cm^{-2}	1.7	> 950 mAh g^{-1} at 2C, 68.8% after 800 cycles	[115]
VN@NC/PP	< 50 mV for 1,000 h at 5 mA cm^{-2}, 0.5 mAh cm^{-2}	2.1	1,134 mAh g^{-1} at 2C, 64% after 1,000 cycles	[117]

lithium dendrites on the anode side[39]. Hwang *et al.* proposed a composite strategy of functionalizing both the composite cathode that consists of sulfur and magnesium-aluminum-layered double hydroxides (MgAl-LDH) combined with CNTs and the asymmetric separator that constructed in sandwich structure with graphene on the cathode side and nano-Al_2O_3 on the anode side, as illustrated in Figure 12A[122]. The MgAl-LDH@CNT-S cathode functions as both an electrocatalyst and polysulfide trap and enhances the reaction kinetics and Coulombic efficiency cycling stability. The modified G/PP/Al_2O_3 separator improves Li^+ and electron transport while preventing undesirable interactions between the cathode and dendritic lithium growth on the anode. Consequently, the Li-S battery demonstrates an impressive initial discharge capacity of 1,330 mAh g^{-1} and retains a high discharge capacity of 730 mAh g^{-1} after 450 cycles at a 1C rate. He reported a flexible Li-S full cell composed of the ultra-stable lithium cloth anode, polysulfone (PSU)-functionalized separator, and freestanding sulfur/graphene/boron nitride nanosheet cathode. The carbon cloth decorated with lithiophilic 3D MnO_2 nanosheets provides excellent flexibility and confines lithium dendrite growth. The functionalized PE separators synthesized with PSU via phase inversion exhibit reduced pore size and enhanced thermal stability. A boron nitride-graphene interlayer is constructed on the cathode surface and functions synergistically with the PSU/PE separator to suppress the shuttle effect [Figure 12B][123].

FUNCTIONALIZED SEPARATORS FOR NA-S BATTERIES

There are significant similarities and distinct differences in the charge/discharge reactions, the sulfur

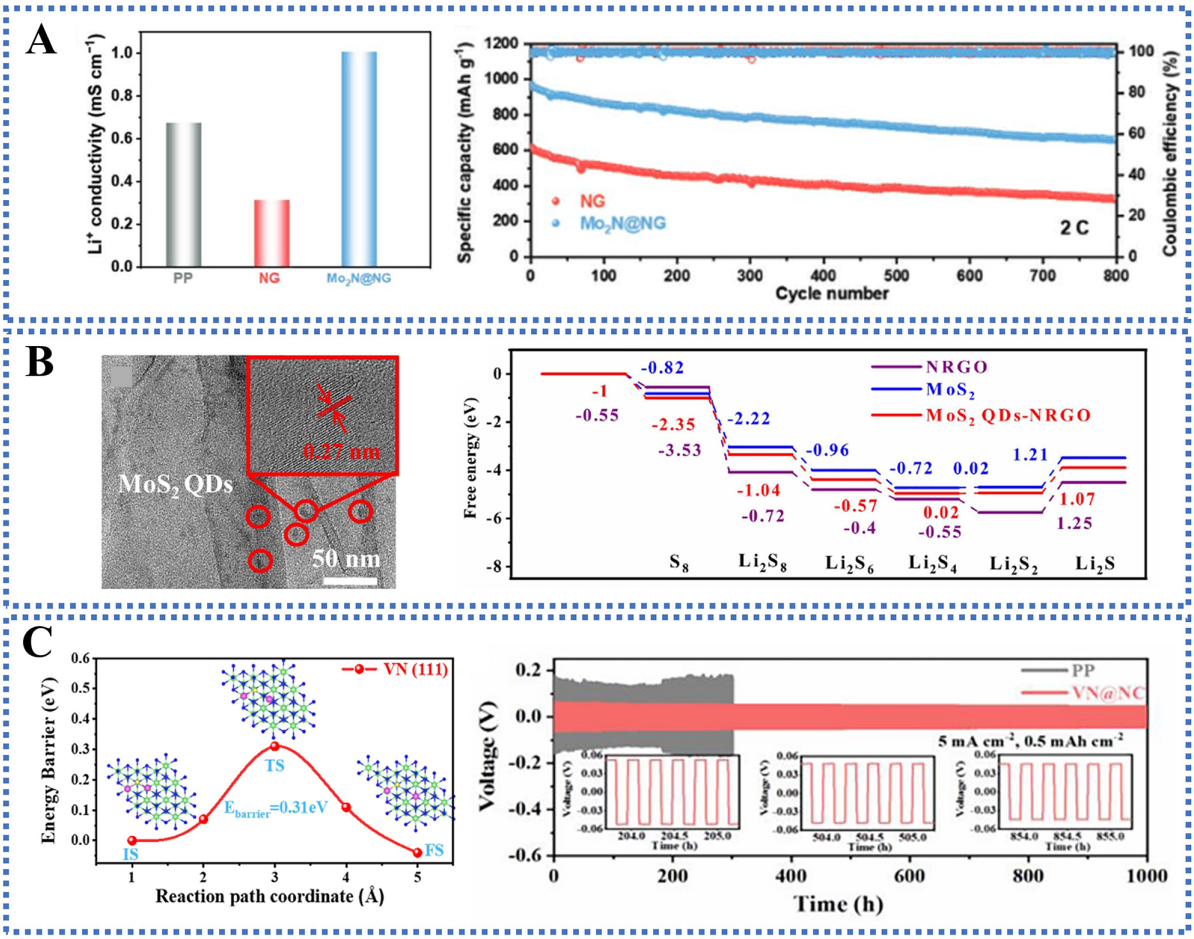

Figure 11. Bifunctional separators with TMBs quantum dots for Li-S batteries. (A) Lithium-ion conductivity and long cycle stability at 2C of the cells with Mo_2N@NG/PP modified separators. (B) TEM, HRTEM images and LiPSs reduction energy profiles of MoS_2 QDs-NRGO. (C) Energy profiles of Li_2S dissociation process on the surface of VN (111) and voltage-time curves of Li-Li symmetric batteries with VN@NC separators. This figure is quoted with permission from Ma *et al.*[115], Zhang *et al.*[116], Ma *et al.*[117], respectively.

cathode structure and the dendrite growth mechanisms of the metal anode in Li-S and Na-S batteries. Similarly, the mechanical barrier capabilities, internal microstructure richness, active site abundance, electrocatalytic ability, electrolyte wettability, and ion conductivity are also effective not only in inhibiting the polysulfide shuttle effect but also in suppressing uncontrolled sodium dendrite growth in Na-S batteries[124]. The development of sulfiphilic and sodiophilic materials is also crucial for Na-S batteries to achieve bifunctional inhibition of polysulfides and sodium dendrite growth at a minimal cost. However, functional separators in Na-S batteries face stricter requirements in terms of mechanical performance, limiting the precipitation of polysulfides in liquid electrolytes, synergizing with solid electrolytes, and assisting in the formation of stable SEI layers[22].

The strategies of replacing traditional separators with new materials and loading functional interlayers are generally conducted on the traditional separators in Na-S batteries: (i) polyolefin separators, including PP and PE; (ii) GF separators; and (iii) Nafion separators, validated for effectiveness for Na-S batteries in 2014[125,126].

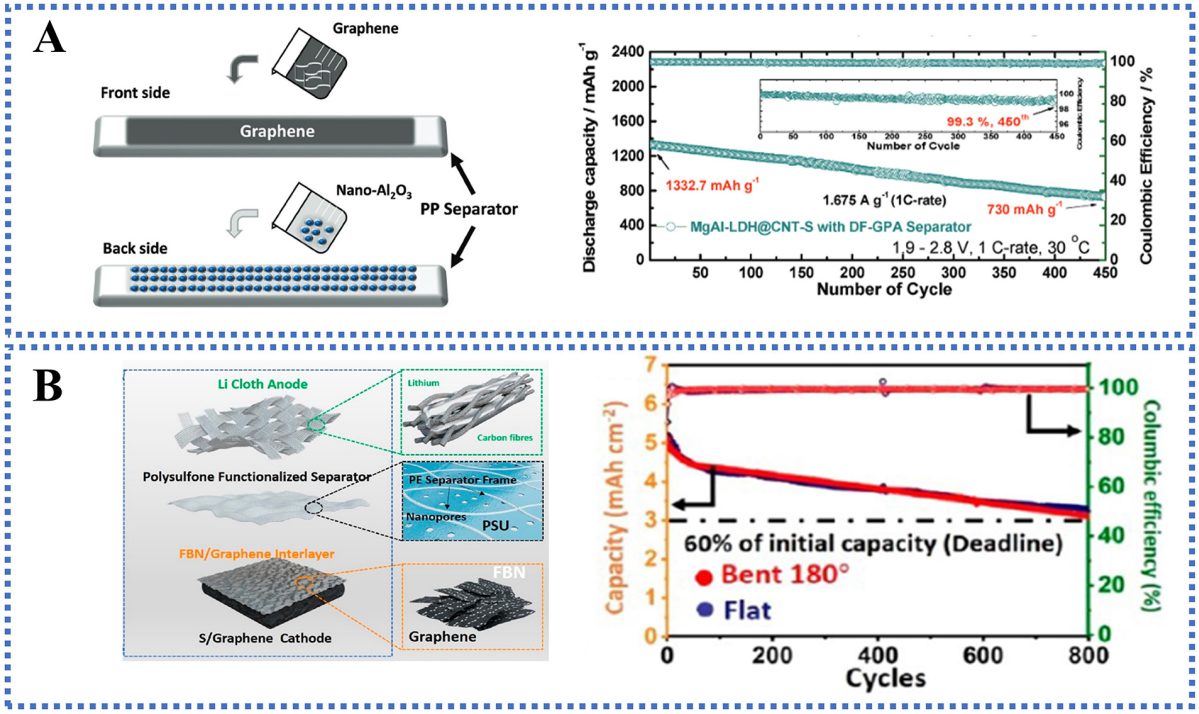

Figure 12. Integrated Strategies for Li-S batteries. (A) Preparation schematic of graphene/PP/Al_2O_3 separator and long-term cycling profiles of the Li-S cell with MgAl-LDH@CNT-S cathode and graphene/PP/Al_2O_3 separator. (B) Schematic of the design and cycling performance of the Li-S full cell. This figure is quoted with permission from Hwang *et al.*[122]. and Yu *et al.*[123], respectively.

Monofunctional separators to inhibit shuttle effect

Similar to Li-S batteries, functionalized separators for Na-S batteries focus on inhibiting the polysulfide shuttle effect through physical confinement, physical/chemical adsorption, and catalytic conversion and sharing similar functional material systems with monofunctional separators of Li-S batteries as summarized in Table 3[21]. The COF with azobenzene side chains in Room-Temperature (RT)/Na-S batteries utilizes the dual functionality of the azobenzene branches, which reduce pore size to the sub-nanometer level and provide active sites for Na^+ adsorption, effectively limiting NaPSs. As shown in Figure 13A, the corresponding RT/Na-S battery demonstrates long-term stable cycling over 1,000 cycles at a rate of 1C[127]. Similarly, functionalized carbon materials are highly ideal for use as intermediate layer materials in Na-S battery separators[128]. Dong *et al.* were the first to employ an eco-friendly composite material of nitrogen and sulfur co-doped carbon nanofibers (derived from waste cigarette filters) and carbon black (N,S-CNF/CB) as an intermediate layer in the GF separator for RT Na-S batteries[129]. The high chemical adsorption capacity of NaPSs by N,S-CNF synergized with the physical adsorption capacity of non-polar CB, limiting the dissolution of NaPSs in the liquid electrolyte as shown in Figure 13B. The RT/Na-S battery with N,S-CNF/CB/GF maintained a substantial discharge capacity of 527 mAh g^{-1} even after 900 cycles at a high rate of 0.5C. In the lightweight 3D cellulose nanofiber-derived carbon aerogel (NSCA@GF), the unique hierarchical porous structure, excellent electronic conductivity, and 3D interconnected network of the N, S co-doped carbon aerogel enhance the NaPSs anchoring capacity of N/S sites, effectively inhibiting the dissolution of NaPSs and improving the kinetics of conversion reactions[130]. In addition, TMCs also exhibit a triple capability for the suppression of polysulfides in Na-S batteries: physical blocking, chemical adsorption, and catalytic activity. Dong *et al.* proposed GF with 2H-$MoSe_2$/nitrogen-doped hollow carbon spheres/GO (2H-$MoSe_2$/N-HCS/GO) coating [Figure 13C] that demonstrated a higher Na^+ transference number and faster Na^+ transport while ensuring NaPSs adsorbing ability[131]. Zhang *et al.* demonstrated that

Table 3. Summary of electrochemical performance of RT-Na-S batteries (coin cell) with monofunctional separators

Separators	Sulfur loading (mg cm^{-2})	Cycling performance	Ref.
Na-Nafion@PP	2	350 mAh g^{-1} at 0.4 mA cm^{-2} after 20 cycles	[125]
Azo-TbTh/GF	1.5	820 mAh g^{-1} at 1C, 63.9% after 1,000 cycles	[127]
N,S-CNF/CB+GF	< 1.2	765 mAh g^{-1} at 0.5C, 68.9% after 900 cycles	[129]
NSCA@GF	1.0-1.5	925.2 mAh g^{-1} at 0.5C, 58.9% after 500 cycles	[130]
2H-$MoSe_2$/N-HCS/GO+GF	1.0-1.45	1,945 mAh g^{-1} at 0.5C, 24.9% after 500 cycles	[131]
Co-NCs/$PW_{10}V_2$@GF	1	825.7 mAh g^{-1} at 10C, 52% after 4,000 cycles	[132]

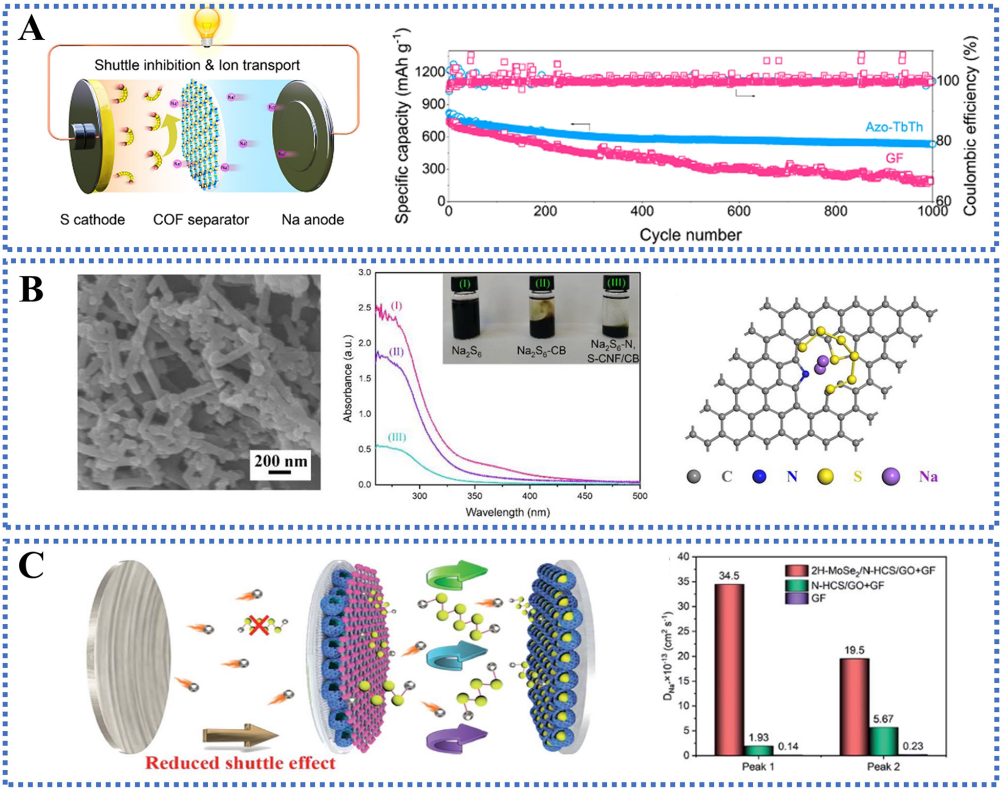

Figure 13. Functional Separator to inhibit shuttle effects for Na-S batteries. (A) Schematic diagram of the Na-S cells with bifunctional COF separators and cycle performance of Azo-TbTh-equipped batteries at 1C. (B) FESEM images of N,S-CNF/CB, UV-vis adsorption spectra of different separators and adsorption configuration for Na_2S_6 on a N,S-CNF surface. (C) Operating process schematic and the enhanced Na^+ diffusion coefficient of RT-Na/S batteries with 2H-$MoSe_2$/N-HCS/GO+GF. This figure is quoted with permission from Yin *et al.*[127], Dong *et al.*[129], and Dong *et al.*[131], respectively.

the heteropolyvanadotungstate $PW_{10}V_2$ can effectively participate in the complete solid-liquid conversion and reversible redox transformation of polysulfides, thereby significantly suppressing the shuttle effect[132].

Bifunctional interlayers on separators

For bifunctional Na-S battery separators, the essential conditions for achieving bifunctionality include enhanced mechanical strength and flexibility, appropriate porosity and micropore size, sufficient ionic and electronic conductivity, and strong Na^+ adsorption energy. The weaker adsorption energy for Na^+ than Li^+ due to the larger ionic radius and lower charge density imposes more stringent requirements on the surface properties and internal chemical bonding of the bifunctional materials.

Functionalized MOF/COF materials can exhibit satisfactory bifunctional effectiveness for Na-S batteries. Chen *et al.* synthesized a self-supporting COF membrane composed of hydroxyl naphthol blue (HB) and CNT (HB/CNT@COF) as shown in Figure 14A[133]. The 3D nanonetwork in COF and CNTs not only provides ample buffering space for the cathode volume changes but also synergizes with the HB containing sulfonic acid groups. The HB/CNT@COF offer excellent ion-sieving capabilities and significantly accelerates electron transfer and reduces interfacial resistance caused by the inert NaPSs layer. Xu *et al.* proposed a functionalized porous ZIF-based membrane (PZM) for RT/Na-S batteries as shown in Figure 14B[134]. The metal ions as Lewis acid centers embedded in the ZIF framework conduct strong chemical bonding with NaPSs anions and attain selective and uniform Na^+ transport in conjunction with the controlled porous structure of the ZIF membrane[134]. Conductive polymers, due to the excellent Na^+ anchoring and transport capabilities, can also serve as bifunctional interlayer additives of Na-S battery separators. Zhou *et al.* developed a single-ion conductive polymer-grafted intermediate layer (PMTFSINa) on the PP separator by a reversible grafting-filtration strategy, achieving a Na^+ transference number (t_{Na+}) of 0.58[135]. However, PMTFSINa exhibits limited ability to suppress the polysulfide shuttle effect and needs cooperation with additional loading of MXene-functionalized low-dimensional materials to improve the NaPSs adsorption.

Unsurprisingly, TMCs are highly suitable for preventing the polysulfide shuttling and sodium dendrite growth on the anode surface in Na-S batteries due to the excellent catalytic properties and conductivity. Wang *et al.* developed an MXene@C nanosheet/PP composite separator with improved electrolyte wettability. Owing to the unique core-shell nanosheet structure shown in Figure 15A, the MXene@C interlayer achieves strong sodium deposition regulation and NaPSs capture capability at an extremely low loading of 0.1 mg cm^{-2} and a thickness of ~1.5 μm[136]. The MXene@C/PP separator exhibits a lower sodium nucleation overpotential of 41.2 mV and faster Na_2S_6 conversion reaction kinetics, as evidenced by smaller voltage polarization and higher current polarization. Sun *et al.* developed amorphous 2D iron tin oxide (A-$FeSnO_x$) nanosheets with hierarchical vacancies and introduced trace amounts (5 wt%) of MXene to ensure sufficient ionic conductivity[137]. The A-$FeSnO_x$ is rich in oxygen vacancies and nanoscale pores and displays higher state density near the Fermi level as shown in Figure 15B[137], indicating improved ionic and electronic conductivity. The A-$FeSnO_x$ also exhibits enhanced polysulfide adsorption and conversion kinetics, particularly for lower-order polysulfides such as Na_2S_2 and Na_2S. The A-$FeSnO_x$@MXene separator facilitates symmetrical Na stripping/deposition behavior for 800 h and stable charge/discharge for up to 400 cycles at 0.5C.

In summary, loading catalytically active polar materials as bifunctional interlayers is the primary method of achieving bifunctional separators for Na-S batteries, as compared in Table 4. However, considering the complex preparation processes and high costs of novel materials such as MXene, research on bifunctional separators for Na-S batteries needs to be conducted towards developing more economical functional materials.

Integrated strategies

Up to now, the reported composite modification strategies for Na-S batteries involving functionalized separators mostly focus on the combination with modified sulfur cathodes[138,139]. Li *et al.* synthesized highly uniform Fe^{3+}/polyacrylamide nanospheres (FPNs) on a large scale as shown in Figure 16A, and then applied mesoporous nitrogen-doped carbon nanospheres (PNC-Ns) obtained by carbonizing FPNs as sulfur hosts and FPNs@graphene composites (FPNs-G) as separator functional interlayers, respectively[140]. The S/PNC-Ns cathode not only enhanced the overall conductivity and mechanical flexibility of the cathode but also accelerated the redox kinetics of polysulfides. It also synergistically worked with the FPNs-G/PP separator to suppress the shuttle effect of NaPSs and improve sulfur utilization. Unfortunately, the

Table 4. Summary of electrochemical performance of RT-Na-S batteries (coin cell) with bifunctional separators

Separators	Cycling performance of Na//Na cell	Sulfur loading (mg cm^{-2})	Cycling performance of Na-S battery	Ref.
HB/CNT@COF	< 150 mV for 300 h at 0.1 mA cm^{-2}	0.5-1	733.4 mAh g^{-1} at 4C after 400 cycles	[133]
PZM@LE	≈50 mV for 400 h at 0.1 mA cm^{-2}, 0.1 mAh cm^{-2}	N/A	≈300 mAh g^{-1} at 0.5C after 800 cycles	[134]
PMTFSINa@DN-MXene/PP	≈100 mV for 500 h at 0.2 mA cm^{-2}	N/A	962 mAh g^{-1} at 0.1C after 200 cycles	[135]
MXene@C/PP/MXene@C	≈50 mV for 800 h at 0.5 mA cm^{-2}, 0.5 mAh cm^{-2}	0.5-0.8	968 mAh g^{-1} at 0.5C 95.8% after 650 cycles	[136]
A-$FeSnO_x$@ MXene/PP	< 100 mV for 800 h at 0.1 mA cm^{-2}, 0.2 mAh cm^{-2}	0.6-1	965.7 mAh g^{-1} at 0.5C 63.2% after 400 cycles	[137]

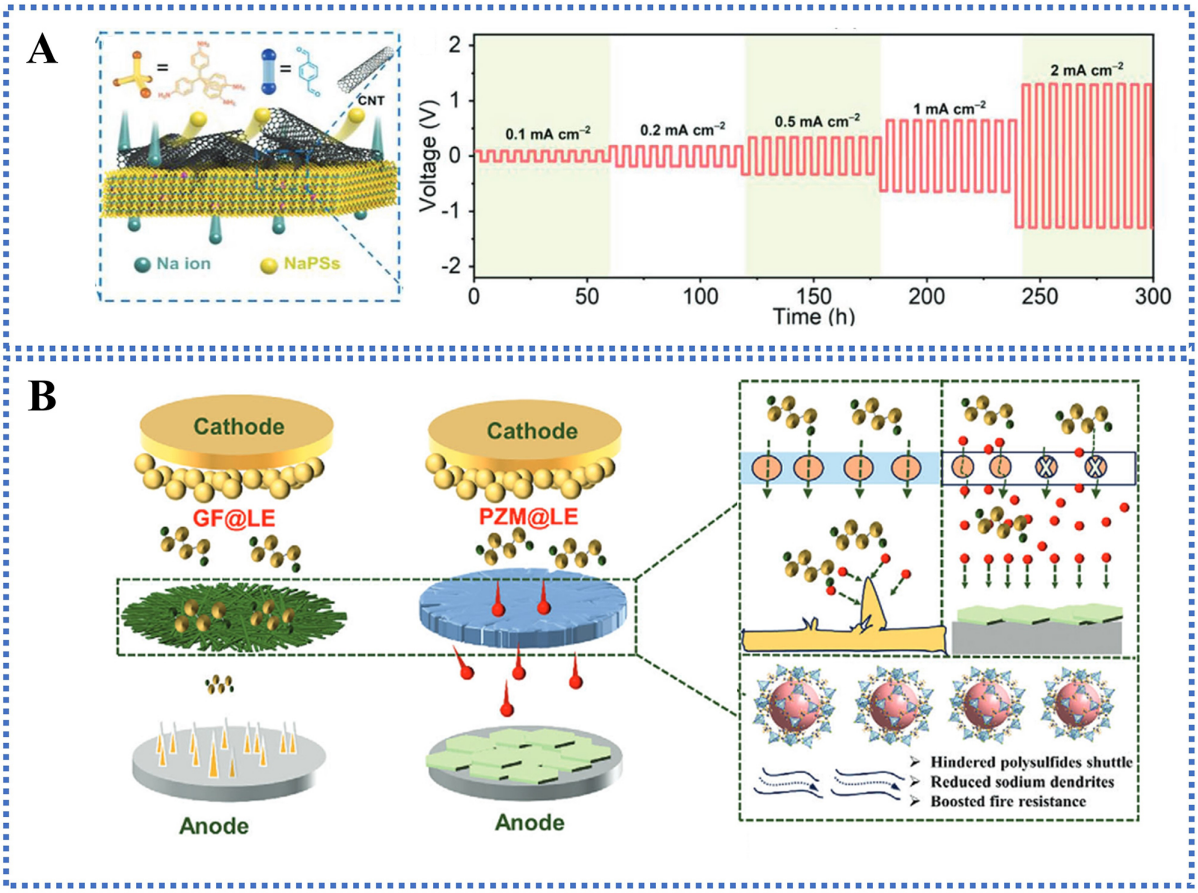

Figure 14. Bifunctional Separator with polar interlayers for Na-S batteries. (A) Selective Na^+ transport mechanism schematic of HB/CNT@COF and voltage rate performances of symmetric Na-S cells with HB/CNT@COF modified separator. (B) Schematic of Na-S batteries equipped with PZM@LE separator. This figure is quoted with permission from Chen *et al.*[133], and Xu *et al.*[134], respectively.

corresponding RT/Na-S separator only maintained a stable capacity of 400 mAh g^{-1} over 800 cycles at 0.5C. Pre-sodiated Nafion separators are also frequently used in composite modification strategies for Na-S batteries. Yu *et al.* prepared a self-woven composite material of high surface area activated carbon (AC) and carbon nanofiber fabric (CNF), referred to as CNF/AC, and conducted it as the conductive matrix for the sulfur cathode [Figure 16B][141]. The highly conductive CNF/AC-S not only facilitated the exchange reaction

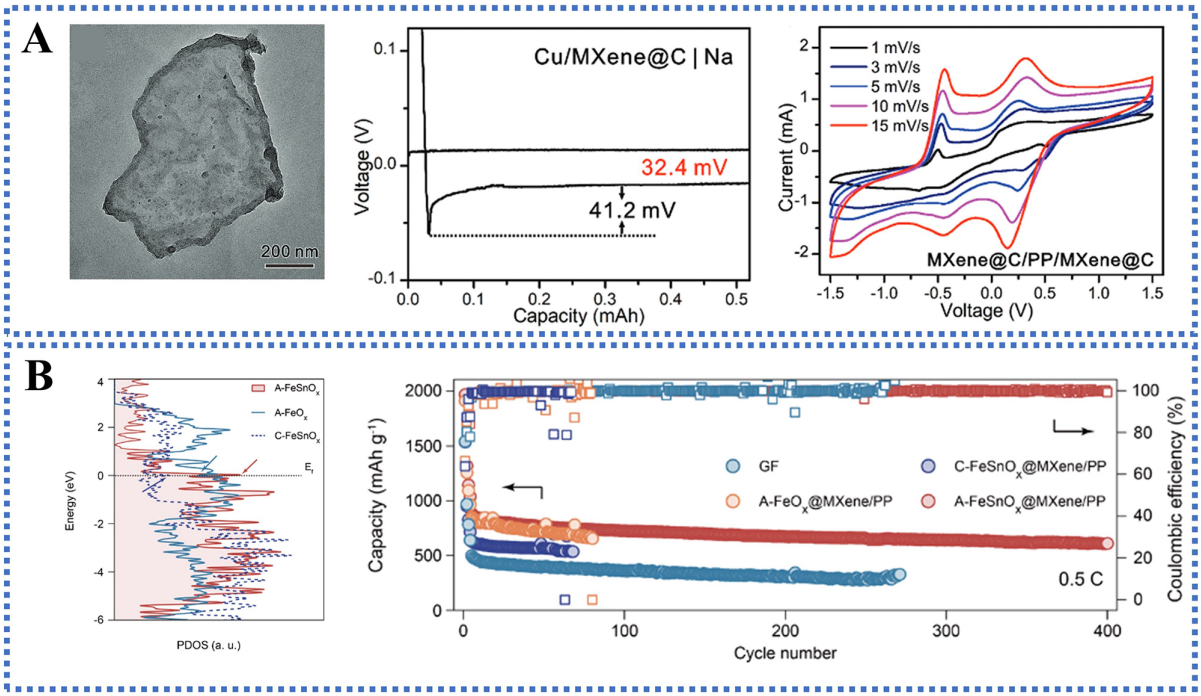

Figure 15. Bifunctional separator with TMBs interlayers for Na-S batteries. (A) TEM image of MXene@C nanosheets, voltage profile of Na-Cu cell and CV curves of the Na-Na symmetric cells with MXene@C separator. (B) Orbital projected density of states analyses for A-$FeSnO_x$ and cycling performance of Na-S cells with different separators at 0.5C. This figure is quoted with permission from Wang *et al.*[136], and Sun *et al.*[137], respectively.

of sodium ions across the pre-sodiated Nafion separator but also offered the advantage of lower manufacturing costs. Besides, the CNF/AC provides satisfactory additional capacity for Na-S batteries.

Although there has been some progress in the exploitation of solid-state electrolytes for Na-S batteries, the strategy of combining electrolyte optimization with separator modification demonstrated limited improvement in cycling performance[29,40]. Overall, an integrated strategy to suppress the shuttle effect and sodium dendrite growth for Na-S batteries remains to be developed. Integrated strategies can maximize the capacity density performance and cycling stability of Na-S batteries. However, balancing the pursuit of higher capacity and lower cost is the greatest focus and challenge for further research.

Functional separators beyond Na-S batteries

Due to the similar electrochemical properties of alkali metal anodes, some specialized functionalized separators have been found to extend beyond Na-S batteries to cover Li-S and even K-S batteries[142]. Chen *et al.* used a universally applicable solid-phase synthesis strategy for MFe@FeO_x (M = Co, Ni, Mn) to synthesize CoFe@FeO_x core-shell nanoparticles uniformly distributed in a carbon matrix[143]. The CoFe@FeO_x functional material, composed of a FeO_x shell with high polysulfide adsorption and a conductive CoFe alloy core, efficiently captures polysulfides and significantly accelerates the conversion rate [Figure 17A][143]. Li-S batteries equipped with CoFe@FeO_x/GF demonstrated stable rate performance at high current densities. The Na-S batteries with CoFe@FeO_x/GF exhibited a cycle life of up to 1,200 cycles with a Coulombic efficiency close to 100%. Li *et al.* effectively captured Li-, Na-, and K-polysulfides by simply introducing SnSe nanosheets into GF [Figure 17B]. The strong adsorption and catalytic ability of SnSe nanosheets for metal polysulfides mainly comes from the unique layered structure that maximizes active site exposure and conductivity[144].

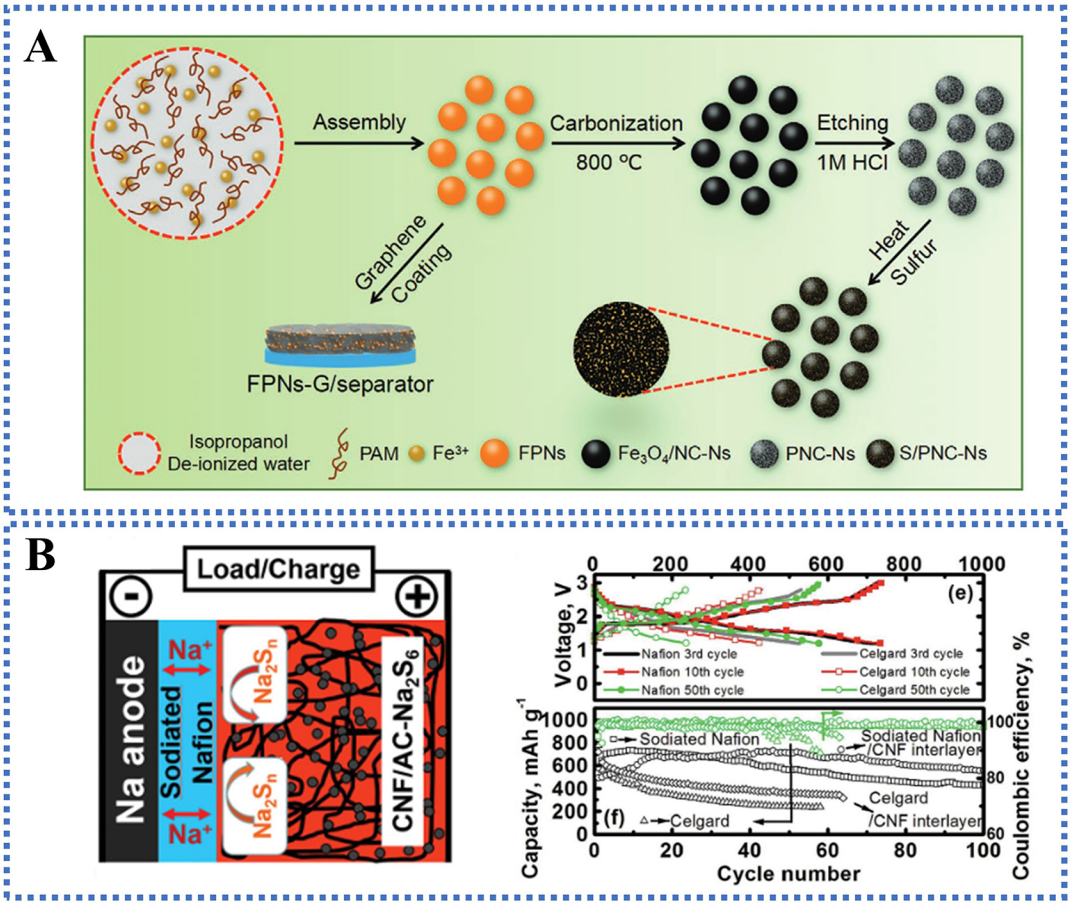

Figure 16. Integrated Strategies for Na-S batteries. (A) Schematic for the FPNs-G/separator fabrication. (B) Schematic and cycling performance of RT Na-S battery with sodiated Nafion separator and CNF/AC composite cathode. This figure is quoted with permission from Li *et al.*[140], and Yu *et al.*[141], respectively.

CONCLUSION AND OUTLOOK

The research on functionalized separators for Li-S and Na-S batteries has made significant progress. This review emphasizes that the polysulfide shuttle effect and the uncontrollable Li/Na dendrite growth on the anode surface are the key issues limiting the advancement of Li/Na-sulfur battery technology. This paper explores and summarizes the optimization key parameters and suppression mechanisms of separators modified with various functional materials, as well as the application of functionalized separators in Li-S and Na-S batteries. The review highlights the potential of coupling functional materials with different mechanisms to improve the comprehensive performance of separators in suppressing the shuttle effect and dendrite growth through synergistic effects.

Researchers have made significant strides in suppressing the polysulfide shuttle effect by developing materials with physical blocking, charge repulsion, and chemical adsorption functions, such as carbon nanomaterials, MOFs and COFs. These materials not only extend the diffusion path of polysulfides in the electrolyte but also provide abundant active sites for the adsorption and conversion of polysulfides. As for suppressing metal dendrite growth, researchers have enhanced the mechanical properties and ion conductivity of separators by incorporating materials with high mechanical strength and excellent electrolyte wettability, such as GFs, PI, and functionalized polymers. These improvements significantly

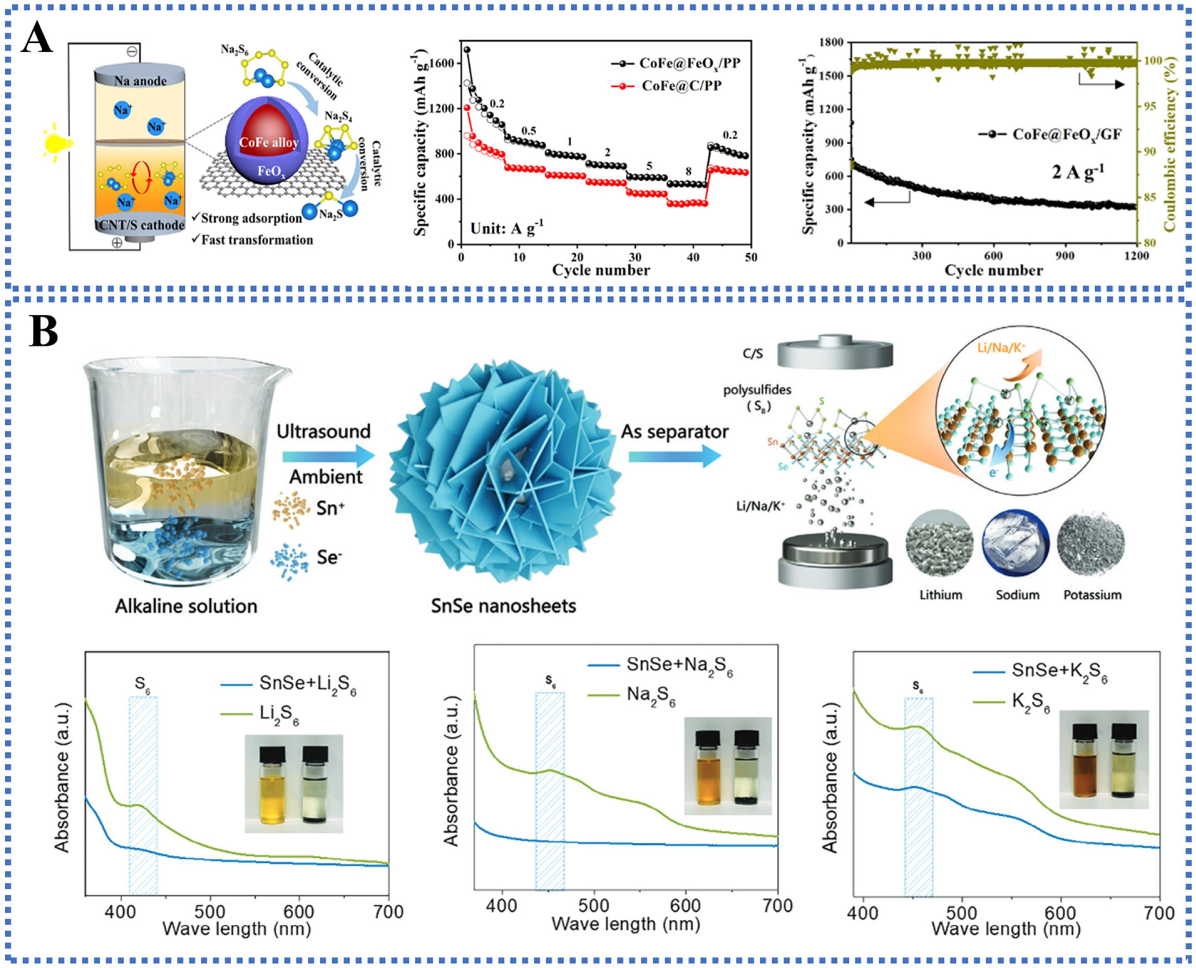

Figure 17. Functional separators beyond Na-S batteries. (A) Mechanism schematic diagram for Na-S battery, rate performance of Li-S battery and long-time cycling performance of Na-S battery of the CoFe@FeO_x catalyst. (B) Schematic synthesis procedure illustration of the SnSe nanosheets, the UV-vis spectra comparison of the Li/Na/K polysulfide solutions with and without SnSe. This figure is quoted with permission from Chen *et al.*[143], and Li *et al.*[144], respectively.

boost the separator's mechanical performance and its ability to suppress dendrite growth. Especially, TMCs have been widely applied in functionalized separators. These materials catalytically convert polysulfides, thereby enhancing the utilization of the sulfur cathode and the cycling stability of the battery. Bifunctional separators are certified to be able to regulate the redox reactions of both the sulfur cathode and the metal anode and achieve effective capture of polysulfides and suppression of metal dendrite growth. Given the crucial role in improving the capacity density and cycling stability of Li/Na-sulfur batteries, functionalized separators are considered one of the most promising optimization strategies for these batteries.

In short, the pursuit of high-capacity and stable Li-S and Na-S batteries has introduced new requirements for functionalized separators, among which dual-functional separators that are capable of suppressing both the polysulfide shuttle effect and uncontrollable Li/Na dendrite growth have increasingly become a critical research focus. In addition to suitable ionic and electronic conductivity, excellent chemical stability, high mechanical strength and moderate flexibility, and the ability to assist in the formation of the stable SEI layer, it is significant for bifunctional separators to possess sulfiphilicity and lithiophilicity/sodiophilicity simultaneously: (i) The strong sulfiphilicity enhances the adsorption capacity of polysulfides and constrains

the migration of polysulfides in the electrolyte, thereby suppressing the shuttle effect; and (ii) The excellent lithiophilicity/sodiophilicity promotes the uniform deposition of lithium/sodium, reducing local electric field enhancement and dendrite growth, thus inhibiting uncontrollable dendrite formation. In comparison to Li-S batteries, the functionalized separators for Na-S batteries are required to have: (i) higher electrolyte compatibility; (ii) more robust capability to suppress the precipitation of lower-order sodium polysulfides that are thermodynamically stable at room temperature; (iii) greater mechanical strength to handle the more pronounced volume changes of the sodium anode during charging/discharging; and (iv) preferably the ability to assist in forming stable SEI layers to mitigate the higher risk of SEI degradation.

However, several challenges still need to be solved for the practical application of functionalized separators in Li-S and Na-S batteries. Firstly, the production costs of high-efficiency functionalized materials (such as certain MOFs and TMCs) are relatively high, and the preparation processes are complex, limiting the large-scale commercial application. Secondly, the long-term cycling stability of functionalized separators needs further validation, especially regarding whether the mechanical properties and chemical stability of the separators are sufficiently reliable under high sulfur loading and high current density conditions. Thirdly, functionalized separators for Na-S batteries still need to be developed. Lastly, existing functionalized separators need help in simultaneously achieving multiple conditions, including battery lightweight, high actual capacity density, long-term safety and stability, and low cost.

In the future, the advancement of separator modifications for Li-S and Na-S batteries may focus on several key areas as follows. First, the development of low-cost and easily scalable functionalized materials is essential to reduce the overall cost of batteries. Secondly, further research and optimization of structural design are needed to achieve uniform distribution and strong adhesion of functional materials on the separator, ensuring stability during long-term cycling. Moreover, the exploration of multifunctional separator designs will comprehensively enhance battery performance, propelling Li-S and Na-S batteries towards higher energy density, longer cycle life, and greater safety.

DECLARATIONS

Authors' contributions

Performed management activities to collect research data for initial use and later reuse, as well as preparation, creation and presentation of the published work, specifically writing the initial draft: Wu, Y.
Performed the preparation of the published work, specifically data visualization: Huang, J.
Performed the preparation of the published work, specifically data collection: Zhang, Z.; Chen, D.; Yu, H.; Ma, F.
Performed the preparation, creation and presentation of the published work by those from the original research group, specifically critical review, commentary or revision including pre-or postpublication stages: Zhang, X.
Performed the preparation, creation and presentation of the published work by those from the original research group, specifically critical review, commentary or revision including pre-or postpublication stages, as well as oversight and leadership responsibility for the research activity planning and execution: Chen, Y.

Availability of data and materials

Not applicable.

Financial support and sponsorship

This research was supported by the open research fund of Songshan Lake Materials Laboratory (2022SLABFN26) and the National Natural Science Foundation of China (21773024).

Conflicts of interest

All authors declared that there are no conflicts of interest.

Ethical approval and consent to participate

Not applicable.

Consent for publication

Not applicable.

Copyright

REFERENCES

1. Tarascon, J. M.; Armand, M. Issues and challenges facing rechargeable lithium batteries. *Nature* **2001**, *414*, 359-67. DOI PubMed
2. Degen, F.; Winter, M.; Bendig, D.; Tübke, J. Energy consumption of current and future production of lithium-ion and post lithium-ion battery cells. *Nat. Energy.* **2023**, *8*, 1284-95. DOI
3. Zhong, Y.; Shi, Q.; Zhu, C.; et al. Mechanistic insights into fast charging and discharging of the sodium metal battery anode: a comparison with lithium. *J. Am. Chem. Soc.* **2021**, *143*, 13929-36. DOI
4. Lei, T.; Chen, W.; Hu, Y.; et al. A nonflammable and thermotolerant separator suppresses polysulfide dissolution for safe and long-cycle lithium-sulfur batteries. *Adv. Energy. Mater.* **2018**, *8*, 1802441. DOI
5. Li, T.; Xu, J.; Wang, C.; Wu, W.; Su, D.; Wang, G. The latest advances in the critical factors (positive electrode, electrolytes, separators) for sodium-sulfur battery. *J. Alloys. Compd.* **2019**, *792*, 797-817. DOI
6. Pan, Y.; Chou, S.; Liu, H. K.; Dou, S. X. Functional membrane separators for next-generation high-energy rechargeable batteries. *Nat. Sci. Rev.* **2017**, *4*, 917-33. DOI
7. Li, Y.; Wang, X.; Wang, L.; et al. Ni@Ni_3N embedded on three-dimensional carbon nanosheets for high-performance lithium/sodium-sulfur batteries. *ACS. Appl. Mater. Interfaces.* **2021**, *13*, 48536-45. DOI
8. Jiang, Y.; Yu, Z.; Zhou, X.; et al. Single-atom vanadium catalyst boosting reaction kinetics of polysulfides in Na-S batteries. *Adv. Mater.* **2023**, *35*, e2208873. DOI
9. Zhou, X.; Yu, Z.; Yao, Y.; et al. A high-efficiency Mo_2 C electrocatalyst promoting the polysulfide redox kinetics for Na-S batteries. *Adv. Mater.* **2022**, *34*, e2200479. DOI
10. Xu, W.; Wang, J.; Ding, F.; et al. Lithium metal anodes for rechargeable batteries. *Energy. Environ. Sci.* **2014**, *7*, 513-37. DOI
11. Zhang, Y.; Wang, J.; Xue, Z. Electrode protection and electrolyte optimization via surface modification strategy for high-performance lithium batteries. *Adv. Funct. Mater.* **2024**, *34*, 2311925. DOI
12. Liu, Z.; Chen, M.; Zhou, D.; Xiao, Z. Scavenging of "dead sulfur" and "dead lithium" revealed by integrated-heterogeneous catalysis for advanced lithium-sulfur batteries. *Adv. Funct. Mater.* **2023**, *33*, 2306321. DOI
13. Wei, Z.; Ren, Y.; Sokolowski, J.; Zhu, X.; Wu, G. Mechanistic understanding of the role separators playing in advanced lithium-sulfur batteries. *InfoMat* **2020**, *2*, 483-508. DOI
14. Hao, H.; Hutter, T.; Boyce, B. L.; Watt, J.; Liu, P.; Mitlin, D. Review of multifunctional separators: stabilizing the cathode and the anode for alkali (Li, Na, and K) metal-sulfur and selenium batteries. *Chem. Rev.* **2022**, *122*, 8053-125. DOI
15. Xu, J.; Qiu, Y.; Yang, J.; et al. Review of separator modification strategies: targeting undesired anion transport in room temperature sodium-sulfur/selenium/iodine batteries. *Adv. Funct. Mater.* **2024**, *34*, 2306206. DOI
16. Xu, R.; Lu, J.; Amine, K. Progress in mechanistic understanding and characterization techniques of Li-S batteries. *Adv. Energy. Mater.* **2015**, *5*, 1500408. DOI
17. Ding, Z.; Tang, Y.; Ortmann, T.; et al. The impact of microstructure on filament growth at the sodium metal anode in all-solid-state sodium batteries. *Adv. Energy. Mater.* **2023**, *13*, 2302322. DOI
18. Wu, J.; Ye, T.; Wang, Y.; et al. Understanding the catalytic kinetics of polysulfide redox reactions on transition metal compounds in Li-S batteries. *ACS. Nano.* **2022**, *16*, 15734-59. DOI
19. Li, C.; Liu, R.; Xiao, Y.; Cao, F.; Zhang, H. Recent progress of separators in lithium-sulfur batteries. *Energy. Storage. Mater.* **2021**, *40*, 439-60. DOI
20. Yu, X.; Manthiram, A. Capacity enhancement and discharge mechanisms of room-temperature sodium-sulfur batteries. *ChemElectroChem* **2014**, *1*, 1275-80. DOI
21. Tang, W.; Aslam, M. K.; Xu, M. Towards high performance room temperature sodium-sulfur batteries: strategies to avoid shuttle effect. *J. Colloid. Interface. Sci.* **2022**, *606*, 22-37. DOI PubMed
22. Lin, L.; Zhang, C.; Huang, Y.; et al. Challenge and strategies in room temperature sodium-sulfur batteries: a comparison with lithium-sulfur batteries. *Small* **2022**, *18*, e2107368. DOI
23. Cooper, E. R.; Li, M.; Gentle, I.; Xia, Q.; Knibbe, R. A deeper understanding of metal nucleation and growth in rechargeable metal

batteries through theory and experiment. *Angew. Chem. Int. Ed.* **2023**, *62*, e202309247. DOI

24. Liu, K.; Zhuo, D.; Lee, H. W.; et al. Extending the life of lithium-based rechargeable batteries by reaction of lithium dendrites with a novel silica nanoparticle sandwiched separator. *Adv. Mater.* **2017**, *29*, 1603987. DOI
25. Brissot, C.; Rosso, M.; Chazalviel, J. N.; Lascaud, S. In situ concentration cartography in the neighborhood of dendrites growing in lithium/polymer-electrolyte/lithium cells. *J. Electrochem. Soc.* **1999**, *146*, 4393-400. DOI
26. Lin, D.; Liu, Y.; Li, Y.; et al. Fast galvanic lithium corrosion involving a Kirkendall-type mechanism. *Nat. Chem.* **2019**, *11*, 382-9. DOI
27. Wang, L.; Wang, T.; Peng, L.; et al. The promises, challenges and pathways to room-temperature sodium-sulfur batteries. *Natl. Sci. Rev.* **2022**, *9*, nwab050. DOI PubMed PMC
28. Li, Z.; Wang, C.; Ling, F.; et al. Room-temperature sodium-sulfur batteries: rules for catalyst selection and electrode design. *Adv. Mater.* **2022**, *34*, e2204214. DOI
29. Kim, I.; Park, J. Y.; Kim, C. H.; et al. A room temperature Na/S battery using a β″ alumina solid electrolyte separator, tetraethylene glycol dimethyl ether electrolyte, and a S/C composite cathode. *J. Power. Sources.* **2016**, *301*, 332-7. DOI
30. Guan, Y.; Wang, A.; Liu, S.; Li, Q.; Wang, W.; Huang, Y. Protecting lithium anode with $LiNO_3$/Al_2O_3/PVDF-coated separator for lithium-sulfur batteries. *J. Alloys. Compd.* **2018**, *765*, 544-50. DOI
31. Chen, M.; Shao, M.; Jin, J.; Cui, L.; Tu, H.; Fu, X. Configurational and structural design of separators toward shuttling-free and dendrite-free lithium-sulfur batteries: a review. *Energy. Storage. Mater.* **2022**, *47*, 629-48. DOI
32. Freitag, A.; Stamm, M.; Ionov, L. Separator for lithium-sulfur battery based on polymer blend membrane. *J. Power. Sources.* **2017**, *363*, 384-91. DOI
33. Zhu, Y.; Zhang, Y.; Jin, S.; et al. Toward safe and high-performance lithium-sulfur batteries via polyimide nanosheets-modified separator. *ACS. Sustain. Chem. Eng.* **2023**, *11*, 1434-47. DOI
34. Yuan, B.; He, N.; Liang, Y.; et al. A surfactant-modified composite separator for high safe lithium ion battery. *J. Energy. Chem.* **2023**, *76*, 398-403. DOI
35. Gu, M.; Wang, J.; Song, Z.; et al. Multifunctional asymmetric separator constructed by polyacrylonitrile-derived nanofibers for lithium-sulfur batteries. *ACS. Appl. Mater. Interfaces.* **2023**, *15*, 51241-51. DOI
36. Zhu, J.; Yanilmaz, M.; Fu, K.; et al. Understanding glass fiber membrane used as a novel separator for lithium-sulfur batteries. *J. Membr. Sci.* **2016**, *504*, 89-96. DOI
37. Li, Y.; Zhu, J.; Zhu, P.; et al. Glass fiber separator coated by porous carbon nanofiber derived from immiscible PAN/PMMA for high-performance lithium-sulfur batteries. *J. Membr. Sci.* **2018**, *552*, 31-42. DOI
38. Wang, P.; Bao, J.; Lv, K.; et al. Rational design of a gel-polymer-inorganic separator with uniform lithium-ion deposition for highly stable lithium-sulfur batteries. *ACS. Appl. Mater. Interfaces.* **2019**, *11*, 35788-95. DOI
39. Bharti, V. K.; Pathak, A. D.; Sharma, C. S.; Khandelwal, M. Flexible and free-standing bacterial cellulose derived cathode host and separator for lithium-sulfur batteries. *Carbohydr. Polym.* **2022**, *293*, 119731. DOI PubMed
40. Zhang, J.; Wang, Y.; Xia, Q.; et al. Confining polymer electrolyte in MOF for safe and high-performance all-solid-state sodium metal batteries. *Angew. Chem. Int. Ed.* **2024**, *63*, e202318822. DOI
41. Yang, K.; Li, C.; Qi, H.; Dai, Y.; Cui, Y.; He, Y. Developing a MXene quantum dot-based separator for Li-S batteries. *J. Mater. Chem. A.* **2023**, *11*, 10425-34. DOI
42. Wang, Y.; Wu, Y.; Mao, P.; et al. A Keggin Al_{13}-montmorillonite modified separator retards the polysulfide shuttling and accelerates Li-ion transfer in Li-S batteries. *Small* **2024**, *20*, e2304898. DOI
43. Kang, X.; He, T.; Zou, R.; et al. Size effect for inhibiting polysulfides shuttle in lithium-sulfur batteries. *Small* **2024**, *20*, e2306503. DOI
44. Razaq, R.; Din, M. M. U.; Småbråten, D. R.; et al. Synergistic effect of bimetallic MOF modified separator for long cycle life lithium-sulfur batteries. *Adv. Energy. Mater.* **2024**, *14*, 2302897. DOI
45. Li, Z.; Zhang, F.; Tang, L.; et al. High areal loading and long-life cycle stability of lithium-sulfur batteries achieved by a dual-function ZnS-modified separator. *Chem. Eng. J.* **2020**, *390*, 124653. DOI
46. Feng, S.; Wang, J.; Wen, J.; et al. Improvement of redox kinetics of dendrite-free lithium-sulfur battery by bidirectional catalysis of cationic dual-active sites. *ACS. Sustain. Chem. Eng.* **2023**, *11*, 8544-55. DOI
47. He, J.; Bhargav, A.; Manthiram, A. Molybdenum boride as an efficient catalyst for polysulfide redox to enable high-energy-density lithium-sulfur batteries. *Adv. Mater.* **2020**, *32*, e2004741. DOI PubMed
48. Zhang, Z.; Xu, Y.; Xiong, D.; et al. Improving sulfur transformation of lean electrolyte lithium-sulfur battery using nickel nanoparticles encapsulated in N-doped carbon nanotubes. *Electron* **2024**, *2*, e19. DOI
49. Nitou, M. V. M.; Pang, Y.; Wan, Z.; et al. $LiFePO_4$ as a dual-functional coating for separators in lithium-ion batteries: a new strategy for improving capacity and safety. *J. Energy. Chem.* **2023**, *86*, 490-8. DOI
50. Hou, Q.; Yu, M.; Jiang, H.; et al. Scalable, flexible and fire-retardant Janus membranes for simultaneously inhibiting dendrite growth and catalyzing polysulfide conversion in lithium-sulfur batteries. *Energy. Storage. Mater.* **2023**, *60*, 102807. DOI
51. Shrshr, A. E.; Dong, Y.; Al-Tahan, M. A.; et al. Modified separator engineering with 2D ultrathin Ni_3B@rGO: extraordinary electrochemical performance of the lithium-sulfur battery with enormous-sulfur-content cathode in low electrolyte/sulfur ratio. *J. Alloys. Compd.* **2022**, *910*, 164917. DOI
52. Cao, Y.; Wu, H.; Li, G.; et al. Ion selective covalent organic framework enabling enhanced electrochemical performance of lithium-

sulfur batteries. *Nano. Lett.* **2021**, *21*, 2997-3006. DOI

53. Huang, Y.; Wang, Y.; Fu, Y. A thermoregulating separator based on black phosphorus/MOFs heterostructure for thermo-stable lithium-sulfur batteries. *Chem. Eng. J.* **2023**, *454*, 140250. DOI
54. Zhang, B.; Qie, J.; Liu, X.; et al. Watermelon flesh-like Ni_3S_2@C composite separator with polysulfide shuttle inhibition for high-performance lithium-sulfur batteries. *Small* **2023**, *19*, e2300687. DOI
55. Chen, L.; Yu, H.; Li, W.; Dirican, M.; Liu, Y.; Zhang, X. Interlayer design based on carbon materials for lithium-sulfur batteries: a review. *J. Mater. Chem. A.* **2020**, *8*, 10709-35. DOI
56. Liu, N.; Huang, B.; Wang, W.; et al. Modified separator using thin carbon layer obtained from its cathode for advanced lithium sulfur batteries. *ACS. Appl. Mater. Interfaces.* **2016**, *8*, 16101-7. DOI
57. Li, B.; Sun, Z.; Zhao, Y.; et al. Functional separator for Li/S batteries based on boron-doped graphene and activated carbon. *J. Nanopart. Res.* **2019**, *21*, 4451. DOI
58. Zeng, P.; Huang, L.; Zhang, X.; Zhang, R.; Wu, L.; Chen, Y. Long-life and high-areal-capacity lithium-sulfur batteries realized by a honeycomb-like N, P dual-doped carbon modified separator. *Chem. Eng. J.* **2018**, *349*, 327-37. DOI
59. Li, Q.; Liu, Y.; Yang, L.; et al. N, O co-doped chlorella-based biomass carbon modified separator for lithium-sulfur battery with high capacity and long cycle performance. *J. Colloid. Interface. Sci.* **2021**, *585*, 43-50. DOI
60. Ma, Z.; Jing, F.; Fan, Y.; Li, J.; Zhao, Y.; Shao, G. High electrical conductivity of 3D mesporous carbon nanocage as an efficient polysulfide buffer layer for high sulfur utilization in lithium-sulfur batteries. *J. Alloys. Compd.* **2019**, *789*, 71-9. DOI
61. Saroha, R.; Heo, J.; Li, X.; et al. Asymmetric separator integrated with ferroelectric-$BaTiO_3$ and mesoporous-CNT for the reutilization of soluble polysulfide in lithium-sulfur batteries. *J. Alloys. Compd.* **2022**, *893*, 162272. DOI
62. Jiang, Y.; Chen, F.; Gao, Y.; et al. Inhibiting the shuttle effect of Li-S battery with a graphene oxide coating separator: performance improvement and mechanism study. *J. Power. Sources.* **2017**, *342*, 929-38. DOI
63. Lin, W.; Chen, Y.; Li, P.; et al. Enhanced performance of lithium sulfur battery with a reduced graphene oxide coating separator. *J. Electrochem. Soc.* **2015**, *162*, A1624-9. DOI
64. Lei, T.; Chen, W.; Lv, W.; et al. Inhibiting polysulfide shuttling with a graphene composite separator for highly robust lithium-sulfur batteries. *Joule* **2018**, *2*, 2091-104. DOI
65. Bai, S.; Liu, X.; Zhu, K.; Wu, S.; Zhou, H. Metal-organic framework-based separator for lithium-sulfur batteries. *Nat. Energy.* **2016**, *1*, 16094. DOI
66. Hall, E. A.; Redfern, L. R.; Wang, M. H.; Scheidt, K. A. Lewis acid activation of a hydrogen bond donor metal-organic framework for catalysis. *ACS. Catal.* **2016**, *6*, 3248-52. DOI
67. Zhang, Y.; Lin, S.; Xiao, J.; Hu, X. Introduced hierarchically ordered porous architecture on a separator as an efficient polysulfide trap toward high-mass-loading Li-S batteries. *ACS. Appl. Mater. Interfaces.* **2024**, *16*, 3888-900. DOI
68. Yu, X.; Wu, H.; Koo, J. H.; Manthiram, A. Tailoring the pore size of a polypropylene separator with a polymer having intrinsic nanoporosity for suppressing the polysulfide shuttle in lithium-sulfur batteries. *Adv. Energy. Mater.* **2020**, *10*, 1902872. DOI
69. Sun, S.; Han, L.; Hou, J.; et al. Single-walled carbon nanotube gutter layer supported ultrathin zwitterionic microporous polymer membrane for high-performance lithium-sulfur battery. *J. Colloid. Interface. Sci.* **2022**, *628*, 1012-22. DOI
70. Tao, X.; Wang, J.; Liu, C.; et al. Balancing surface adsorption and diffusion of lithium-polysulfides on nonconductive oxides for lithium-sulfur battery design. *Nat. Commun.* **2016**, *7*, 11203. DOI PubMed PMC
71. Yang, Y.; Huang, X.; Cao, Z.; Chen, G. Thermally conductive separator with hierarchical nano/microstructures for improving thermal management of batteries. *Nano. Energy.* **2016**, *22*, 301-9. DOI
72. Lin, Z.; Xu, J.; Lei, Y.; et al. Enhanced Li-S battery performance boosted by a large surface area mesoporous alumina-based interlayer. *ACS. Appl. Energy. Mater.* **2022**, *5*, 15615-23. DOI
73. Zhang, Y. C.; Li, Y. W.; Han, C.; et al. Ultrathin MgB_2 nanosheet-modified polypropylene separator for high-efficiency lithium-sulfur batteries. *J. Colloid. Interface. Sci.* **2024**, *653*, 664-72. DOI
74. Wu, T.; Yang, T.; Zhang, J.; et al. CoB and BN composites enabling integrated adsorption/catalysis to polysulfides for inhibiting shuttle-effect in Li-S batteries. *J. Energy. Chem.* **2021**, *59*, 220-8. DOI
75. Liang, Q.; Wang, S.; Yao, Y.; Dong, P.; Song, H. Transition metal compounds family for Li-S batteries: the DFT-guide for suppressing polysulfides shuttle. *Adv. Funct. Mater.* **2023**, *33*, 2300825. DOI
76. Huang, Y.; Lin, L.; Zhang, Y.; et al. Dual-functional lithiophilic/sulfiphilic binary-metal selenide quantum dots toward high-performance Li-S full batteries. *Nanomicro. Lett.* **2023**, *15*, 67. DOI PubMed PMC
77. Sun, L.; Zhang, W.; Fu, J.; et al. Highly active rare earth sulfur oxides used for membrane modification of lithium sulfur batteries. *Chem. Eng. J.* **2023**, *457*, 141240. DOI
78. Zuo, Y.; Zhu, Y.; Tang, X.; et al. MnO_2 supported on acrylic cloth as functional separator for high-performance lithium-sulfur batteries. *J. Power. Sources.* **2020**, *464*, 228181. DOI
79. Zhu, W.; Zhang, Z.; Wei, J.; et al. A synergistic modification of polypropylene separator toward stable lithium-sulfur battery. *J. Membr. Sci.* **2020**, *597*, 117646. DOI
80. Zhu, H.; Dong, S.; Xiong, J.; et al. MOF derived cobalt-nickel bimetallic phosphide (CoNiP) modified separator to enhance the polysulfide adsorption-catalysis for superior lithium-sulfur batteries. *J. Colloid. Interface. Sci.* **2023**, *641*, 942-9. DOI
81. He, J.; Chen, Y.; Manthiram, A. Vertical Co_9S_8 hollow nanowall arrays grown on a Celgard separator as a multifunctional polysulfide barrier for high-performance Li-S batteries. *Energy. Environ. Sci.* **2018**, *11*, 2560-8. DOI

82. Ghazi, Z. A.; He, X.; Khattak, A. M.; et al. MoS_2/celgard separator as efficient polysulfide barrier for long-life lithium-sulfur batteries. *Adv. Mater.* **2017**, *29*, 1606817. DOI
83. Fan, B.; He, Q.; Wei, Q.; Liu, W.; Zhou, B.; Zou, Y. Anchoring and catalyzing polysulfides by rGO/MoS_2/C modified separator in lithium-sulfur batteries. *Carbon* **2023**, *214*, 118361. DOI
84. Zhou, X.; Cui, Y.; Huang, X.; Zhang, Q.; Wang, B.; Tang, S. Interface engineering of Fe_3Se_4/FeSe heterostructures encapsulated in MXene for boosting LiPS conversion and inhibiting shuttle effect. *Chem. Eng. J.* **2023**, *457*, 141139. DOI
85. Wang, M.; Zhu, Y.; Sun, Y.; et al. A universal graphene-selenide heterostructured reservoir with elevated polysulfide evolution efficiency for pragmatic lithium-sulfur battery. *Adv. Funct. Mater.* **2023**, *33*, 2211978. DOI
86. Zhang, J.; Cheng, Y.; Chen, H.; et al. MoP quantum dot-modified N,P-carbon nanotubes as a multifunctional separator coating for high-performance lithium-sulfur batteries. *ACS. Appl. Mater. Interfaces.* **2022**, *14*, 16289-99. DOI
87. Qiu, W.; An, C.; Yan, Y.; et al. Suppressed polysulfide shuttling and improved Li^+ transport in Li S batteries enabled by NbN modified PP separator. *J. Power. Sources.* **2019**, *423*, 98-105. DOI
88. Zhang, J.; Wang, Y.; Zhou, Z.; Chen, Q.; Tang, Y. Mo_2C-loaded porous carbon nanosheets as a multifunctional separator coating for high-performance lithium-sulfur batteries. *Materials* **2023**, *16*, 1635. DOI PubMed PMC
89. Pan, H.; Tan, Z.; Zhou, H.; et al. Fe_3C-N-doped carbon modified separator for high performance lithium-sulfur batteries. *J. Energy. Chem.* **2019**, *39*, 101-8. DOI
90. Ma, F.; Yu, B.; Zhang, X.; et al. $WN_{0.67}$-embedded N-doped graphene-nanosheet Interlayer as efficient polysulfide catalyst and absorbant for high-performance lithium-sulfur batteries. *Chem. Eng. J.* **2022**, *431*, 133439. DOI
91. Ma, F.; Chen, Y. Mo_2N quantum dots decorating N-doped carbon nanosheets for kinetics-enhanced Li-S batteries. *Surf. Interfaces.* **2023**, *42*, 103521. DOI
92. Li, Y. X.; Feng, Y. S.; Li, L. X.; Yin, X.; Cao, F. F.; Ye, H. Green synthesis and applications of MXene for lithium-sulfur batteries. *Energy. Storage. Mater.* **2024**, *67*, 103257. DOI
93. Li, Y.; Li, Z.; Zhou, C.; et al. Gradient sulfur fixing separator with catalytic ability for stable lithium sulfur battery. *Chem. Eng. J.* **2021**, *422*, 130107. DOI
94. Guan, B.; Zhang, Y.; Fan, L.; et al. Blocking polysulfide with Co_2B@CNT via "synergetic adsorptive effect" toward ultrahigh-rate capability and robust lithium-sulfur battery. *ACS. Nano.* **2019**, *13*, 6742-50. DOI
95. Jin, L.; Ni, J.; Shen, C.; et al. Metallically conductive TiB_2 as a multi-functional separator modifier for improved lithium sulfur batteries. *J. Power. Sources.* **2020**, *448*, 227336. DOI
96. Wang, Y.; Wang, P.; Yuan, J.; et al. Binary sulfiphilic nickel boride on boron-doped graphene with beneficial interfacial charge for accelerated Li-S dynamics. *Small* **2023**, *19*, e2208281. DOI
97. Ponraj, R.; Kannan, A. G.; Ahn, J. H.; et al. Effective trapping of lithium polysulfides using a functionalized carbon nanotube-coated separator for lithium-sulfur cells with enhanced cycling stability. *ACS. Appl. Mater. Interfaces.* **2017**, *9*, 38445-54. DOI
98. Li, H.; Zhou, Y.; Zhao, M.; et al. Suppressed shuttle via inhibiting the formation of long-chain lithium polysulfides and functional separator for greatly improved lithium-organosulfur batteries performance. *Adv. Energy. Mater.* **2020**, *10*, 1902695. DOI
99. Wu, S.; Yao, Y.; Nie, X.; Yu, Z.; Yu, Y.; Huang, F. Interfacial engineering of binder-free janus separator with ultra-thin multifunctional layer for simultaneous enhancement of both metallic Li anode and sulfur cathode. *Small* **2022**, *18*, e2202651. DOI
100. Chang, C.; Yang, C.; Wu, Q.; et al. All-in-one Janus separator for lithium-sulfur batteries with lithium polysulfide and dendrite growth suppressed at temperature gradient effect. *J. Power. Sources.* **2022**, *550*, 232115. DOI
101. Dang, B.; Gao, D.; Luo, Y.; Zhang, Z.; Li, J.; Wu, F. Bifunctional design of cerium-based metal-organic framework-808 membrane modified separator for polysulfide shuttling and dendrite growth inhibition in lithium-sulfur batteries. *J. Energy. Storage.* **2022**, *52*, 104981. DOI
102. Chen, X.; Huang, Y.; Li, J.; et al. Bifunctional separator with sandwich structure for high-performance lithium-sulfur batteries. *J. Colloid. Interface. Sci.* **2020**, *559*, 13-20. DOI
103. Xiang, Y.; Wang, Z.; Qiu, W.; et al. Interfacing soluble polysulfides with a SnO_2 functionalized separator: an efficient approach for improving performance of Li-S battery. *J. Membr. Sci.* **2018**, *563*, 380-7. DOI
104. Wang, B.; Guo, W.; Fu, Y. Anodized aluminum oxide separators with aligned channels for high-performance Li-S batteries. *ACS. Appl. Mater. Interfaces.* **2020**, *12*, 5831-7. DOI
105. Liu, J.; Duan, C.; Hong, Z.; et al. Interfacial polymerization achieved integration of pore size adjustment, electrostatic repulsion and physical adsorption into one to inhibit polysulfide shuttle for enhanced lithium-sulfur battery. *J. Power. Sources.* **2024**, *594*, 233975. DOI
106. Wu, J.; Zeng, H.; Li, X.; et al. Ultralight layer-by-layer self-assembled MoS_2-polymer modified separator for simultaneously trapping polysulfides and suppressing lithium dendrites. *Adv. Energy. Mater.* **2018**, *8*, 1802430. DOI
107. Liu, H.; Wang, X.; Wang, Q.; Pei, C.; Wang, H.; Guo, S. Dual-functional cobalt phosphide nanoparticles for performance enhancement of lithium-sulfur battery. *J. Nanostruct. Chem.* **2024**, *14*, 281-92. DOI
108. Li, Y.; Wang, Z.; Gu, H.; Jia, H.; Long, Z.; Yan, X. Niobium boride/graphene directing high-performance lithium-sulfur batteries derived from favorable surface passivation. *ACS. Nano.* **2024**, *18*, 8863-75. DOI
109. Pu, J.; Wang, T.; Tan, Y.; Fan, S.; Xue, P. Effect of heterostructure-modified separator in lithium-sulfur batteries. *Small* **2023**, *19*, e2303266. DOI PubMed
110. Wang, X.; Deng, N.; Liu, Y.; et al. Porous and heterostructured molybdenum-based phosphide and oxide nanobelts assisted by the

structural engineering to enhance polysulfide anchoring and conversion for lithium-sulfur batteries. *Chem. Eng. J.* **2022**, *450*, 138191. DOI

111. Lv, Y.; Bai, L.; Jin, Q.; et al. VSe_2/V_2C heterocatalyst with built-in electric field for efficient lithium-sulfur batteries: Remedies polysulfide shuttle and conversion kinetics. *J. Energy. Chem.* **2024**, *89*, 397-409. DOI
112. Liang, Q.; Wang, S.; Lu, X.; et al. High-entropy MXene as bifunctional mediator toward advanced Li-S full batteries. *ACS. Nano.* **2024**, *18*, 2395-408. DOI
113. Yao, Y.; Wang, S.; Jia, X.; et al. Freestanding sandwich-like hierarchically TiS_2-TiO_2/Mxene bi-functional interlayer for stable Li-S batteries. *Carbon* **2022**, *188*, 533-42. DOI
114. Ma, F.; Zhang, X.; Sriniva, K.; et al. NbN nanodot decorated N-doped graphene as a multifunctional interlayer for high-performance lithium-sulfur batteries. *J. Mater. Chem. A.* **2022**, *10*, 8578-90. DOI
115. Ma, F.; Srinivas, K.; Zhang, X.; et al. Mo_2N quantum dots decorated N-doped graphene nanosheets as dual-functional interlayer for dendrite-free and shuttle-free lithium-sulfur batteries. *Adv. Funct. Mater.* **2022**, *32*, 2206113. DOI
116. Zhang, J.; Hu, J.; Li, X.; et al. High-performance MoS_2 quantum dots/graphene functionalized separator and its failure analysis under high sulfur loading. *Chem. Eng. J.* **2023**, *456*, 140972. DOI
117. Ma, F.; Chen, Z.; Srinivas, K.; et al. VN quantum dots anchored N-doped carbon nanosheets as bifunctional interlayer for high-performance lithium-metal and lithium-sulfur batteries. *Chem. Eng. J.* **2023**, *459*, 141526. DOI
118. Zhang, Y.; Guo, C.; Zhou, J.; et al. Anisotropically hybridized porous crystalline Li-S battery separators. *Small* **2023**, *19*, e2206616. DOI
119. Wu, H.; Jiang, M.; Gao, X.; et al. All-in-one Janus covalent organic frameworks separator as fast Li nucleator and polysulfides catalyzer in lithium-sulfur batteries. *J. Colloid. Interface. Sci.* **2024**, *662*, 138-48. DOI
120. Wang, Z.; Feng, L.; Deng, C.; Wang, S. 2,5-Dimercapto-1,3,4-thiadiazole/acetylene black@polypropylene separator for inhibiting the shuttle effect and electrocatalyzing electrode reactions in Li-S batteries. *Chem. Eng. J.* **2022**, *446*, 137153. DOI
121. Li, R.; Li, J.; Wang, X.; et al. Surface design for high ion flux separator in lithium-sulfur batteries. *J. Colloid. Interface. Sci.* **2024**, *654*, 13-24. DOI
122. Hwang, J. Y.; Kim, H. M.; Shin, S.; Sun, Y. K. Designing a high-performance lithium-sulfur batteries based on layered double hydroxides-carbon nanotubes composite cathode and a dual-functional graphene-polypropylene-Al_2O_3 separator. *Adv. Funct. Mater.* **2018**, *28*, 1704294. DOI
123. Yu, B.; Fan, Y.; Mateti, S.; et al. An ultra-long-life flexible lithium-sulfur battery with lithium cloth anode and polysulfone-functionalized separator. *ACS. Nano.* **2021**, *15*, 1358-69. DOI
124. Zhang, J.; Zhang, G.; Chen, Z.; et al. Emerging applications of atomic layer deposition for lithium-sulfur and sodium-sulfur batteries. *Energy. Stor. Mater.* **2020**, *26*, 513-33. DOI
125. Bauer, I.; Kohl, M.; Althues, H.; Kaskel, S. Shuttle suppression in room temperature sodium-sulfur batteries using ion selective polymer membranes. *Chem. Commun.* **2014**, *50*, 3208-10. DOI PubMed
126. Wang, Y.; Zhang, Y.; Cheng, H.; et al. Research progress toward room temperature sodium sulfur batteries: a review. *Molecules* **2021**, *26*, 1535. DOI PubMed PMC
127. Yin, C.; Li, Z.; Zhao, D.; et al. Azo-branched covalent organic framework thin films as active separators for superior sodium-sulfur batteries. *ACS. Nano.* **2022**, *16*, 14178-87. DOI
128. Kumar Saroja AP, Xu Y. Carbon materials for Na-S and K-S batteries. *Matter* **2022**, *5*, 808-36. DOI
129. Dong, C.; Zhou, H.; Liu, H.; et al. Inhibited shuttle effect by functional separator for room-temperature sodium-sulfur batteries. *J. Mater. Sci. Technol.* **2022**, *113*, 207-16. DOI
130. Yang, W.; Yang, W.; Zou, R.; et al. Cellulose nanofiber-derived carbon aerogel for advanced room-temperature sodium-sulfur batteries. *Carbon. Energy.* **2023**, *5*, e203. DOI
131. Dong, C.; Zhou, H.; Jin, B.; et al. Enabling high-performance room-temperature sodium/sulfur batteries with few-layer 2H-$MoSe_2$ embellished nitrogen-doped hollow carbon spheres as polysulfide barriers. *J. Mater. Chem. A.* **2021**, *9*, 3451-63. DOI
132. Zhang, J.; Zhang, X.; Wang, J.; et al. The explicit multi-electron catalytic mechanism of heteropolyvanadotungstate dominating ultra-durable room-temperature Na-S batteries. *Adv. Funct. Mater.* **2024**, *34*, 2400170. DOI
133. Chen, S.; Liang, L.; Li, Y.; et al. Brain capillary-inspired self-assembled covalent organic framework membrane for sodium-sulfur battery separator. *Adv. Energy. Mater.* **2023**, *13*, 2204334. DOI
134. Xu, H.; Xiang, Y.; Xu, X.; et al. A polysulfides-defensive, dendrite-suppressed, and flame-retardant separator with lean electrolyte for room temperature sodium-sulfur batteries. *Adv. Funct. Mater.* **2024**, 2403663. DOI
135. Zhou, D.; Tang, X.; Guo, X.; et al. Polyolefin-based janus separator for rechargeable sodium batteries. *Angew. Chem. Int. Ed.* **2020**, *59*, 16725-34. DOI
136. Wang, C.; Wu, K.; Cui, J.; Fang, X.; Li, J.; Zheng, N. Robust room-temperature sodium-sulfur batteries enabled by a sandwich-structured MXene@C/polyolefin/MXene@C dual-functional separator. *Small* **2022**, *18*, e2106983. DOI
137. Sun, W.; Hou, J.; Zhou, Y.; et al. Amorphous $FeSnO_x$ nanosheets with hierarchical vacancies for room-temperature sodium-sulfur batteries. *Angew. Chem. Int. Ed.* **2024**, *63*, e202404816. DOI
138. Yu, X.; Manthiram, A. Performance enhancement and mechanistic studies of room-temperature sodium-sulfur batteries with a carbon-coated functional Nafion separator and a Na_2S/activated carbon nanofiber cathode. *Chem. Mater.* **2016**, *28*, 896-905. DOI
139. Wang, H.; Deng, C.; Li, X.; et al. Designing dual-defending system based on catalytic and kinetic iron Pyrite@C hybrid fibers for

long-life room-temperature sodium-sulfur batteries. *Chem. Eng. J.* **2021**, *420*, 129681. DOI

140. Li, H.; Zhao, M.; Jin, B.; Wen, Z.; Liu, H. K.; Jiang, Q. Mesoporous nitrogen-doped carbon nanospheres as sulfur matrix and a novel chelate-modified separator for high-performance room-temperature Na-S batteries. *Small* **2020**, *16*, e1907464. DOI
141. Yu, X.; Manthiram, A. Ambient-temperature sodium-sulfur batteries with a sodiated Nafion membrane and a carbon nanofiber-activated carbon composite electrode. *Adv. Energy. Mater.* **2015**, *5*, 1500350. DOI
142. Fang, Y.; Zhang, Y.; Zhu, K.; et al. Lithiophilic three-dimensional porous $Ti_2C_3T_x$-rGO membrane as a stable scaffold for safe alkali metal (Li or Na) anodes. *ACS. Nano.* **2019**, *13*, 14319-28. DOI
143. Chen, Y.; Yao, Y.; Zhao, W.; et al. Precise solid-phase synthesis of CoFe@FeO_x nanoparticles for efficient polysulfide regulation in lithium/sodium-sulfur batteries. *Nat. Commun.* **2023**, *14*, 7487. DOI PubMed PMC
144. Li, C.; Yang, D.; Yu, J.; et al. Three birds with one stone: multifunctional separators based on SnSe nanosheets enable high-performance Li-, Na- and K-sulfur batteries. *Adv. Energy. Mater.* **2024**, *14*, 2303551. DOI